Time Course Analysis of Gene Expression During Light-Induced Photoreceptor Cell Death and Regeneration in *albino* Zebrafish

Sean C. Kassen,[1,2] Vijay Ramanan,[1,2] Jacob E. Montgomery,[1,2] Christopher T. Burket,[1,2] Chang-Gong Liu,[3]* Thomas S. Vihtelic,[1,2]† David R. Hyde,[1,2]

[1] Department of Biological Sciences, University of Notre Dame, Notre Dame, Indiana 46556

[2] Center for Zebrafish Research, University of Notre Dame, Notre Dame, Indiana 46556

[3] Kimmel Cancer Center, Thomas Jefferson University, Philadelphia, Pennsylvania 19107

Received 22 June 2006; revised 22 September 2006; accepted 17 October 2006

ABSTRACT: **Constant intense light causes apoptosis of rod and cone photoreceptors in adult *albino* zebrafish. The photoreceptors subsequently regenerate from proliferating inner nuclear layer (INL) progenitor cells that migrate to the outer nuclear layer (ONL) and differentiate into rods and cones. To identify gene expression changes during this photoreceptor regeneration response, a microarray analysis was performed at five time points during the light treatment. The time course included an early time point during photoreceptor death (16 h), later time points during progenitor cell proliferation and migration (31, 51, and 68 h) and a 96 h time point, which likely corresponds to the initial photoreceptor differentiation. Mean expression values for each gene were calculated at each time point relative to the control (0 h light exposure) and statistical analysis by one-way ANOVA identified 4567 genes exhibiting significant changes in gene expression along the time course. The genes within this data set were clustered based on their temporal expression patterns and proposed functions. Quantitative real-time PCR validated the microarray expression profiles for selected genes, including *stat3* whose expression increased markedly during the light exposure. Based on immunoblots, both total and activated Stat3 protein expression also increased during the light treatment. Immunolocalization of Stat3 on retinal tissue sections demonstrated increased expression in photoreceptors and Müller glia by 16 h of light exposure. Some of the Stat3-positive Müller cells expressed PCNA at 31 h, suggesting that Stat3 may play a role in signaling a subset of Müller cells to proliferate during the regeneration response.**
Develop Neurobiol 67: 1009–1031, 2007

Keywords: **retinal regeneration; adult stem cell; microarray; zebrafish; Stat3**

INTRODUCTION

The teleost retina is a well-established model system for determining the cellular and molecular basis of neuronal regeneration (Raymond and Hitchcock, 1997; Hitchcock and Raymond, 2004). A variety of lesion paradigms including surgical excision, toxin injection, laser-induced photocoagulation, localized heat application and exposure to intense light have been employed to damage different retinal cell classes in various fish species (Braisted and Ray-

This article contains supplementary material available via the Internet at http://www.interscience.wiley.com/jpages/1932-8451/suppmat.

**Present address:* Department of Molecular Virology, Immunology and Medical Genetics, The Ohio State University, Columbus, Ohio 43210.

†Contributed to all aspects of this study including preparation of the manuscript.

Correspondence to: D.R. Hyde (dhyde@nd.edu).

Contract grant sponsor: NIH; contract grant number: R21EY017134.

Contract grant sponsor: Center for Zebrafish Research.

Published online 6 March 2007 in Wiley InterScience (www.interscience.wiley.com).
DOI 10.1002/dneu.20362

mond, 1992; Hitchcock et al., 1992; Braisted et al., 1994; Cameron and Easter, 1995; Vihtelic and Hyde, 2000; Wu et al., 2001; Raymond et al., 2006). While all cell types in the zebrafish retina can be regenerated, significant damage to the photoreceptor layer may be required to initiate the response (Braisted and Raymond, 1992; Cameron and Easter, 1995; Raymond et al., 1988; Cameron and Carney, 2000; Yurco and Cameron, 2005). The regenerated cells differentiate from a proliferating progenitor cell population that likely arises from Müller glial cells within the inner nuclear layer (INL), with subsequent migration to their respective laminar locations (Hitchcock et al., 1992; Vihtelic and Hyde, 2000; Wu et al., 2001; Faillace et al., 2002; Yurco and Cameron, 2005; Fausett and Goldman, 2006; Raymond et al., 2006).

Adult teleost retinas maintain a population of INL stem cells that provide new rod photoreceptors during the persistent retinal growth that characterizes teleost fish (Julian et al., 1998; Otteson et al., 2001). In addition, the other retinal cell types are generated from a stem cell population at the retinal margin where annular growth occurs (Johns, 1977, 1982; Raymond et al., 2006). Under normal conditions, the postembryonic stem cells within these two different retinal compartments must divide asymmetrically to both self renew and provide a source of progenitors to feed the various retinal cell lineages. Subsequent to their birth within the INL, the progenitor cells migrate to the outer nuclear layer (ONL) to become rod precursor cells, which also exhibit mitotic activity and ultimately differentiate into rod photoreceptors. Thus, the rod precursor cells likely represent a population of transit amplifying cells, which have been identified in other adult-generated neuronal lineages (Beites et al., 2005). While the Pax6 transcription factor is expressed in a subpopulation of mitotically active INL cells, NeuroD expression marks the teleost ONL rod precursor cells (Otteson et al., 2001; Faillace et al., 2002; Hitchcock and Kakuk-Atkins, 2004). However, the complete complement of molecular markers defining the different retinal precursor subtypes in the adult teleost retina has not been identified.

INL cell proliferation and the generation of new retinal progenitors is up-regulated upon injury to the teleost retina. Intense light exposure of *albino* zebrafish causes widespread photoreceptor cell death in the dorsal retina within 24 h, which appears to initiate the photoreceptor regeneration response (Vihtelic and Hyde, 2000; Vihtelic et al., 2005). Proliferating cells in the INL are detected by PCNA immunohistochemistry after 24 h of light exposure and many clusters of dividing fusiform-shaped cells are observed 72 h after light treatment initiation (Vihtelic and Hyde, 2000). The INL cells generated during this phase of massive cell proliferation migrate to the ONL within 96 h after light exposure initiation and begin to differentiate into rod and cone photoreceptors (Vihtelic and Hyde, 2000; Wu et al., 2001). During this time, the Müller glial cells undergo a variety of changes. The Müller cells exhibit signs of hypertrophy and the migrating retinal progenitors remain in association with the Müller cell radial processes. In addition, protein expression changes characterize many of these glial cells (Vihtelic and Hyde, 2000; Vihtelic et al., 2005; Yurco and Cameron, 2005). Thus, the different phases of the light-lesion-induced retinal response, such as cell death, INL cell proliferation and migration, and Müller glial cell changes are histologically and immunohistochemically definable and largely occur during the first 4 days after light exposure initiation. The characterization of the cellular response to the light-lesion provides a framework for examining the global transcriptional changes associated with this neural cell regeneration response.

To identify gene expression changes associated with photoreceptor regeneration in zebrafish, we performed a time course microarray analysis. RNA was isolated from pooled retinas collected at five different time points representing key events of retinal damage and regeneration that occur within the first 96 h after light exposure initiation. Fluorescent-labeled cDNA was synthesized from the RNA harvested at each time point and hybridized to arrays containing the Compugen/Sigma-Genosis 17K zebrafish oligo set. Statistical analysis identified 4567 genes that exhibited significant changes in gene expression along the time course. To facilitate the identification of candidates for further study, the genes within this data set were clustered based on their temporal expression patterns and proposed functions. Quantitative real-time PCR validated the microarray expression profiles for selected genes. This time course analysis of gene expression during photoreceptor regeneration complements the gene expression profiles that were determined subsequent to surgical lesion of the zebrafish retina (Cameron et al., 2005). Furthermore, these studies will help to elucidate conditions within the molecular niche responsible for adult neural stem cell stimulation and the mechanisms regulating their proliferation, migration and differentiation into different photoreceptor cell types.

METHODS

Animals and Light-Lesion Protocol

Adult *albino*^{b4} zebrafish (*Danio rerio*) were raised under normal facility lights (300 lux; 14 h light:10 h dark) in the University of Notre Dame Zebrafish Facility according to

established protocols (Westerfield, 1993). The zebrafish were dark-treated for 12 days and subjected to constant intense light (2800 lux) using four 150-W halogen lamps (Vihtelic et al., 2005). Retinas were examined at 0, 16, 31, 51, 68, and 96 h of light exposure. Control animals (0 h intense light exposure) of the same age and genotype were raised under normal facility light conditions. The *albino* fish used for histological, immunohistochemical and quantitative real-time PCR analyses were 7–9 months post-fertilization (pf), while the *albino* zebrafish used for microarray analysis were all 20–24 months pf. Prior to enucleation, fish were deeply anesthetized in 0.2% 2-phenoxyethanol and killed by anesthetic overdose. All experimental protocols were approved by the animal use committee at the University of Notre Dame and were in compliance with the ARVO statement for the use of animals in vision research.

Histology

Control and light-lesioned eyes were fixed in 0.1 *M* cacodylate/2.5% glutaraldehyde/2% formaldehyde for 24 h at 4°C. Eyes were processed, embedded in PolyBed 812, sectioned (2.5 μm) and stained with 0.5% methylene blue/0.5% azure II as previously described (Vihtelic et al., 2005). Images were taken of the most severely damaged dorsal retinal region (Vihtelic et al., 2005).

Polyclonal Antiserum Generation, Immunohistochemistry, and Immunoblot Analysis

The carboxyl terminal 118 amino acids of zebrafish Stat3 was expressed as a bacterial fusion protein using the pET32a vector (Novagen, San Diego, CA). This region of Stat3 possesses the least amino acid identity compared to the other Stat proteins identified in zebrafish (Stat3, NP_571554; Stat1, NP_571555; Stat4, NP_001004510; Stat5.1, NP_919368; Stat5.2, NP_001003984). The fusion protein was purified using S-protein agarose and was used to immunize rabbits (Proteintech Group, Chicago, IL). A second Stat3 fusion protein was generated as a T7-tag fusion protein by cloning the Stat3 cDNA sequence corresponding to the carboxyl terminal 118 amino acids into the pET21a vector (Novagen). This T7 fusion protein was expressed, purified using T7 agarose, and coupled to the column matrix according to the manufacturer protocol (AminoLink Coupling Gel; Pierce Biotechnology, Rockford, IL). The anti-Stat3 rabbit serum was immunopurified over this column.

For opsin (Vihtelic et al., 1999) and PCNA (Sigma, St. Louis, MO) immunohistochemistry, the control and light-lesioned eyes were fixed in ethanolic formaldehyde overnight at 4°C (Vihtelic and Hyde, 2000). The eyes were washed in 5% sucrose/PBS (pH 7.4), placed into 20% sucrose/PBS overnight at 4°C, infiltrated in 20% sucrose/PBS:OCT (1:1) for 4 h at room temperature and frozen embedded in OCT. The eye frozen sections were immunolabeled as previously described (Vihtelic and Hyde, 2000). Immunohistochemistry using monoclonal antibody to HuC/D (Molecular Probes, Eugene, OR), the mouse monoclonal to glutamine synthetase (Chemicon, Temecula, CA), or the affinity-purified Stat3 antiserum that we generated, was performed in an identical manner, except the eyes were fixed in 4% paraformaldehyde/5% sucrose/PBS for 2 h at room temperature. The secondary antibodies were Alexa Fluor-488, -568 or -594 conjugates (Molecular Probes).

Total retinal protein for immunoblot analysis was harvested from control and light-lesioned fish by homogenizing 8 retinas in extraction buffer (PBS [pH 7.4]/1% Triton X-100) and incubating on ice for 1 h. The total protein equivalent of 0.1 retina for each time point was combined with 4X sample loading buffer and 10X reducing buffer (Invitrogen, Carlsbad, CA). The sample was incubated at 70°C for 10 min, electrophoresed through a 4%–12% SDS-PAGE (Invitrogen), and transferred to PVDF. The membrane was blocked (PBS/5% nonfat dry milk/0.1% Tween-20) and incubated with the affinity-purified rabbit polyclonal Stat3 antiserum (1:5000), the rabbit polyclonal pStat-727 (1:1000; MBL International, Woburn, MA), the rabbit polyclonal pStat-705 (1:300; Cell Signaling Technology), or a mouse monoclonal anti-actin (clone JLA20; 1:10,000; CalBiochem, San Diego, CA). This actin antibody recognizes the α-, β-, and γ-actin isoforms. The ECL-Plus detection system (Amersham Biosciences, Piscataway, NJ) was used to visualize primary antibody binding.

Microarray Experimental Design, Hybridization, and Statistical Analysis

A total of 66 adult (20–24 months post-fertilization) *albino* zebrafish were used for the time course microarray analysis. Gene expression within the *albino* retinas was examined at 16, 31, 51, 68, and 96 h of intense light exposure and compared to a non-light-treated control group (0 h intense light). Seven to 10 fish were subjected to the intense light for each period of time and total RNA was extracted from the pooled retinas of each treatment group using the RiboPure Kit (Ambion, Austin, TX). The RNA was eluted in water and concentrated by vacuum centrifugation. The RNA concentration, purity, and integrity were assessed by measuring the absorbance at 260 and 280 nm and by gel electrophoresis. Fluorescent-labeled cDNA was synthesized for each time point and hybridized individually to arrays containing the Compugen/Sigma-Genosis 17K zebrafish oligo sets by the Thomas Jefferson University (TJU) Microarray Core Facility (http://www.KimmelCancerCenter.org). Three technical replicates were performed for each time point by hybridizing each of the labeled cDNA samples to three independent arrays. Signal detection, array scanning and the raw data from these hybridizations were compiled by the TJU microarray service. For array gene annotation, visit http://www.labonweb.com.

Signal intensities were quantified for all the genes on the microarray. Total intensity normalization by median was applied to the raw microarray data for each spot, and mean expression values for each gene at each time point were calculated relative to the control. The data was $\log_2$-transformed in preparation for further statistical analysis using GeneSifter (http://www.genesifter.net). A one-way analysis of variance (ANOVA) was applied to isolate genes showing significant ($p_{adj} = 0.05$) up- or down-regulation during the time course, using the Bonferroni step-down procedure to correct for any artificial *p*-value inflation. Genes demonstrating significant changes in expression along the time course were then grouped according to their known functions using GeneSifter. In addition, the interactive hierarchical clustering software GeneXplorer was used to group these genes based on distinct temporal expression patterns (Jiang et al., 2003).

Quantitative Real-Time PCR

The microarray results were validated by quantitative real-time PCR of 12 selected genes using an ABI PRISM 7700 Sequence Detector (Applied Biosystems, Foster City, CA). Total RNA (RNAqueous Kit, Ambion) was extracted from 8 retinas at the same time points examined in the microarray experiment (0, 16, 31, 51, 68, and 96 h light exposure). Thus, the material for real-time PCR analysis was collected from a different set of fish than was used for the gene array analysis. The RNA was concentrated by vacuum centrifugation and cDNA was reverse transcribed using random hexamers (SuperScript First Strand Synthesis System, Invitrogen). The gene-specific primers for the various target genes were designed using the ABI Primer Express program (Applied Biosystems; *rhodopsin*, NM_131084; *green opsin* (*opn1mw2*), NM_182891; *ash*(*a*), U14587; *vimentin*, NM_131872; *pax6a*, NM_131304; *carbonic anhydrase*, BC065611; *p27*, BC064282; *gfap*, NM_131373; *glutamine synthetase 1*, BK000047; *glutamine synthetase 2*, BK000048; *olig2*, NM_178100; *stat3*, NM_131479). The protocols for sample preparation and run conditions described in the ABI 7700 user manual were followed (Applied Biosystems). Briefly, SYBR Green master mix (Applied Biosystems) was combined with the various primer pairs (3 μL of each primer at 5 μM each) and cDNA (1 μL) in a total volume of 50 μL. The reactions were heated for 2 min at 50°C and 10 min at 95°C followed by 40 cycles of 15 s at 95°C and 1 min at 60°C. Agarose gel electrophoresis and dissociation curve analysis subsequent to the amplifications verified that single products were produced with each of the primer pairs used in these experiments.

The comparative C_T method was used for data analysis (Johnson et al., 2000; Vong et al., 2003). Two types of preliminary validation experiments were performed to ensure the applicability of this analysis method for each of the genes examined. First, we determined the suitability of the 18s rRNA gene as an internal reference for data normalization in the light-damaged and regenerating zebrafish retinal tissue. For this experiment, cDNA corresponding to each of the time points was quantified by fluorometric assay (Turner Biosystems, Sunnyvale, CA). Equal amounts of cDNA template from each time point were used for real-time PCR amplification and consistent C_T values for each of the samples were obtained, which verified the stability of 18S rRNA gene expression during the experimental time course. Second, we determined that the amplification efficiency for each target gene compared with the 18S rRNA gene was approximately equal (Johnson et al., 2000; Vong et al., 2003). To determine the amplification efficiencies, the differences in the C_T values between each target gene and the 18S rRNA reference gene (ΔC_T) were obtained for at least three template dilutions. An equation of the line obtained when the template input amount was plotted against ΔC_T indicated that the slope was less than or equal to 0.1 in nearly all cases, although a few genes with very low expression levels had slightly greater slopes (Johnson et al., 2000).

For each gene examined during the light-treatment time course by qRT-PCR, serial dilutions of cDNA from each of the time points were run in triplicate and the median C_T value was normalized against the corresponding median 18S rRNA C_T values, which were also obtained for each time point. The normalized C_T values for each gene from each light treatment time point were compared to the non-light-treated control to obtain the $\log_2$-fold change in gene expression levels.

Tg(*gfap*:*EGFP*)^{nt} Transgenic Line

The 1538 bp immediately upstream of the *glial fibrillary acidic protein* (*gfap*) translational start codon was PCR amplified from AB genomic DNA (Platinum Taq DNA Polymerase High Fidelity; Invitrogen). The forward (5′-CTCGAGGCTACACTTGTACCCAATCAAGG-3′) and reverse (5′-GGATCCGGTGGAGGAGAATGAGATCGAG-3′) primers included *Bam*HI and *Xho*I restriction sites, respectively. PCR products were A-tailed and cloned into the pCR2.1-TOPO vector (Invitrogen). The promoter was subcloned into pT2KXIG (Kawakami et al., 1998), upstream of the EGFP gene within the defective Tol2 element, using the *Xho*I and *Bam*HI restriction sites.

Plasmid DNA for injection was purified using the QIAGEN Plasmid Maxi Kit (QIAGEN; Valencia, CA), extracted with phenol:chloroform (1:1), precipitated with ethanol, and resuspended in nuclease-free water. Tol2 transposase was transcribed *in vitro* from pCSTZ2.8 plasmid DNA and prepared as described (Thummel et al., 2005). The pT2KXIG expression construct and *in vitro* transcribed Tol2 mRNA were combined at a concentration of 25 ng/μL each and injected into two and four-cell stage embryos. Founders were identified by out-crossing F_0 adults and screening the progeny for EGFP expression. Independent transgenic lines were generated from F_1 transgene carriers. Expression of EGFP in the Müller glia of transgenic animals was confirmed by immunolabeling adult retina frozen sections with anti-glutamine synthetase.

RESULTS

Histological Analysis of the Light-Damaged Retinas

To survey gene expression changes during the photoreceptor regeneration response in zebrafish, we selected a series of time points based on previous histological and immunohistochemical characterizations that represented different phases of light-induced damage and photoreceptor regeneration in *albino* zebrafish (Vihtelic and Hyde, 2000; Vihtelic et al., 2005). This time course included an early time point during photoreceptor cell death (16 h light exposure) and relatively evenly spaced time points during progenitor cell proliferation and migration (31, 51, and 68 h light exposure). Since the regenerated rod and cone cells arise from these proliferating INL cells, an additional time point (96 h light exposure) was also selected, which likely corresponds to the initial stage of photoreceptor differentiation.

Histology was used to further define the cell morphological changes that characterize the light-lesioned retinas at each of these time points (Fig. 1). The three nuclear and two plexiform layers of the zebrafish retina are evident in the control section [Fig. 1(A)]. The organized layers of cone ellipsoids and long rod outer segments are also easily visualized in the control. At 16 h of light exposure, the rod outer segments appear swollen and their parallel arrangement is disturbed [Fig. 1(B)]. In addition, the density of nuclei in the ONL appears reduced compared with that of the control. Some ONL nuclei may be pyknotic at this time point because large numbers of TUNEL-positive cells are present in the light-damaged zebrafish retina at 12–16 h of light exposure (Vihtelic and Hyde, 2000). These histological changes and data from previous studies suggest that photoreceptor cell death is initiated within 16 h of exposure to the intense light.

At 31 h, the photoreceptor layer is more disorganized compared with the 16 h time point and the retinal pigmented epithelial cells are vacuolated [Fig. 1, compare (C) and (B)]. The cone ellipsoid layers are less defined relative to the control. In addition, spaces between the INL cells are apparent, which suggests there may be some retinal cell reorganization. At 51 and 68 h of light exposure, the number of ONL nuclei appear much less than the control and no rod outer segment structures are identified using light microscopy [Fig. 1(D,E), respectively]. Furthermore, the outer plexiform layer (OPL) is less defined at 68 h compared with the earlier time points. Therefore, the histological analysis suggests that between 16 and 68 h after light exposure initiation, the majority of photoreceptors are lost and significant structural reorganization is underway.

At 96 h, the light-damaged retinas are characterized by severe photoreceptor layer pathology and morphological changes in the INL [Fig. 1(F)]. The ONL nuclei are larger and more elongated compared to the nuclei in the ONL of the control. Also, the region of the photoreceptor layer normally containing the rod outer segments now consists of large cells and debris. The identity of these cells is unknown, but they may be macrophages, retinal pigmented epithelium (RPE) cells, or glial cells that migrated into the area (Wu et al., 2001). The inner retinal layers display columns of cells that are organized around or within the Müller glial cells (Vihtelic and Hyde, 2000; Vihtelic et al., 2005; Fausett and Goldman, 2006). These glial cells span from the ganglion cell layer (GCL) to the ONL and their radial processes are apparent within the IPL, which is different from the control. These histological changes are consistent with previous data, which demonstrates the ONL is repopulated with cells that either migrated from the INL or arose through ONL cell proliferation (Vihtelic and Hyde, 2000; Faillace et al., 2002; Otteson and Hitchcock, 2003). In addition, the Müller cells undergo complex phenotypic changes in response to the severe photoreceptor layer damage (Vihtelic et al., 2005; Yurco and Cameron, 2005).

Rod and Cone Degeneration Is Closely Followed by INL Cell Proliferation

High levels of INL cell proliferation coincide spatially with the most severely damaged photoreceptors of the superior (dorsal) retinal region (Vihtelic et al., 2005). To examine the time course of cell proliferation and correlate the INL changes with the overlying light-induced photoreceptor damage, PCNA immunolocalization was combined with opsin immunohistochemistry (Fig. 2). The rhodopsin protein level at 16 h of light exposure appears reduced relative to the control [Fig. 2, compare (B) and (A)]. The rhodopsin signal continues to decrease through 68 h of light treatment and is largely undetectable by 96 h [Fig. 2(C–F)]. Thus, rhodopsin protein declines during the light-induced photoreceptor cell death and the lack of detectable rhodopsin protein by 96 h of light exposure correlates with the lack of histologically detectable photoreceptors at this time.

The reduction in green opsin protein expression during the course of intense light exposure is rela-

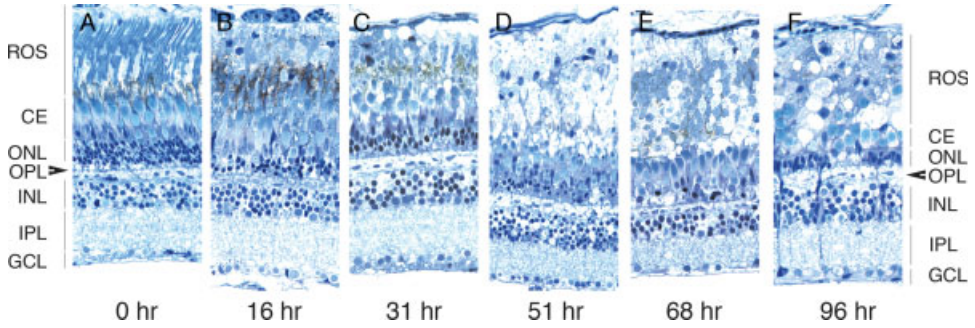

Figure 1

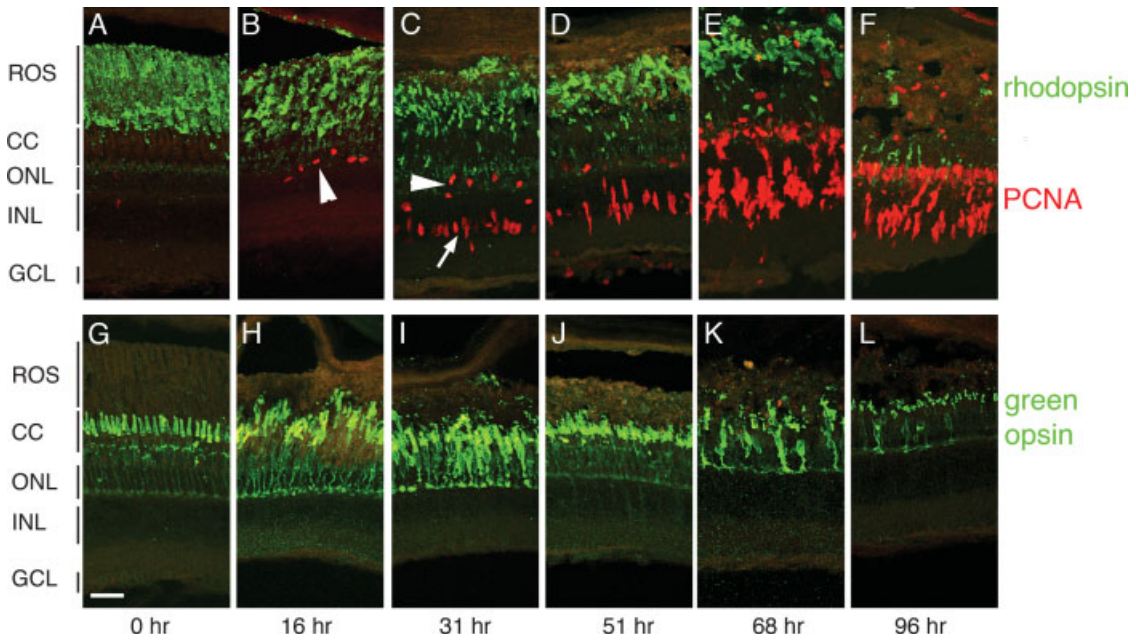

Figure 2

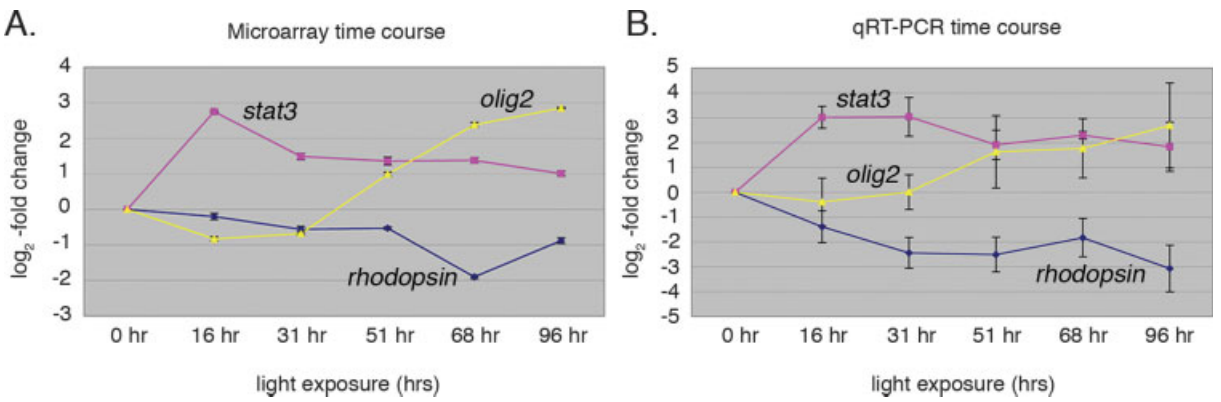

Figure 3

tively similar to the reduction in rhodopsin during this time, although the variability in the degree of cone destruction between retinas suggests that cone cell loss is less consistent than the widespread rod cell death (data not shown). At 16 and 31 h [Fig. 2(H,I), respectively], the green cones appear disor-

ganized compared with the control and the green opsin protein begins to be mislocalized to the inner segments and synaptic pedicles. By 68 and 96 h, only a few intact green cones are identified and the remaining cones exhibit aberrant morphologies [Fig. 2(K,L) respectively]. The changes in rod and cone photoreceptor morphology and opsin mislocalization during the first 96 h of light exposure are consistent with light-induced damage. Although some light-lesioned retinas retain a few intact green cone cells and others exhibit nearly complete cone cell loss, the time course of rod and cone demise that results from the intense light exposure is similar.

Zebrafish regenerate photoreceptors from INL cells, which begin to proliferate subsequent to the light-induced photoreceptor damage (Vihtelic and Hyde, 2000; Vihtelic et al., 2005). PCNA immunohistochemistry was used to visualize the magnitude and location of proliferating cells within the retina during the intense light exposure [Fig. 2(A–F), red signal]. At 16 h, increased numbers of PCNA-positive cells were observed in the ONL [Fig. 2(B), arrowhead]. Increased INL cell proliferation was first identified at 31 h after light treatment initiation, which is later than the photoreceptor damage as demonstrated by histology and immunohistochemistry [Fig. 2(C)]. At 31 h, the majority of PCNA-positive cells were within the distal (vitreal) aspect of the INL. This proliferating INL cell population consists mostly of individual cells with slightly elongated nuclei and a few PCNA-labeled cells were also located within the ONL [Fig. 2(C), arrow and arrowhead, respectively]. At 51 h, the INL PCNA-positive cells were clustered and many exhibited a more fusiform morphology compared to the 31 h time point [Fig. 2, compare (D) with (C)]. In addition, PCNA-positive cells spanned the outer plexiform layer, which is consistent with their migration from the INL to the ONL [Fig. 2(D,E)]. At 68 and 96 h, the INL exhibited large numbers of PCNA-positive cell clusters, which

Figure 1 Histology of the light-damaged zebrafish retina. Dark-treated adult *albino* zebrafish were exposed to constant light for 0–96 h. Plastic retinal sections were stained with 1% methylene blue/azure II. The control section (0 h) displays intact ROS and the ONL is several nuclei thick. At 16 h of light exposure, the ROS are swollen and the ONL nuclei density appears decreased. By 31 h of light, the ROS are reduced in length compared to the control and the ONL is only one nucleus thick. At 51–96 h, the outer segments are severely disrupted, the ONL nuclei are elongated and the OPL is difficult to discern. Abbreviations: ROS, rod outer segments; CE, cone ellipsoids; ONL, outer nuclear layer; OPL, outer plexiform layer; INL, inner nuclear layer; IPL, inner plexiform layer; GCL, ganglion cell layer. Scale bar represents 25 μm.

Figure 2 Rhodopsin, PCNA and green opsin immunolocalization during light exposure. Frozen retinal sections were labeled with polyclonal anti-rhodopsin to visualize the rod outer segments (green signal, A–F), monoclonal anti-PCNA (red signal, A–F) to detect proliferating cells, and polyclonal anti-green opsin to visualize the green cone photoreceptors (green signal, G–L). Rhodopsin protein decreases through the time course, which coincides with the death of most rod photoreceptors. PCNA-positive cells are visible in the ONL (arrowhead) at 16 h and are first detected in the INL (arrow) at 31 h of light exposure. By 51 h, fusiform-shaped PCNA-labeled cells are detected in the INL and large numbers of PCNA-positive cells are observed in the ONL, INL and OPL at 68 and 96 h of light exposure. Green opsin protein is mislocalized to the cone photoreceptor cell bodies and axons at 16 and 31 h. Green opsin expression appears decreased at 51–68 h relative to the control. By 96 h, cone outer segment length and green opsin expression appear severely reduced relative to the control. Abbreviations: ROS, rod outer segments; CE, cone ellipsoids; ONL, outer nuclear layer; OPL, outer plexiform layer; INL, inner nuclear layer; IPL, inner plexiform layer; GCL, ganglion cell layer. Scale bar represents 25 μm.

Figure 3 Comparison of microarray and qRT-PCR gene expression profiles. The time courses of the gene expression changes as determined by the microarray analysis (A) and quantitative real-time PCR (qRT-PCR; Panel B). In (A), the increased expression of *stat3* and *olig2* contrasts with the reduction in *rhodopsin* transcript levels during the light exposure time course. The qRT-PCR expression profiles for *stat3*, *olig2* and *rhodopsin* (B) appear very similar to the microarray-based profile. The $\log_2$ of the mean expression is plotted for the microarray data, while $\log_2$ of the mean ($n = 3$) is plotted for the qRT-PCR.

Table 1 Quantitative RT-PCR Gene Expression Analysis

Gene	Light Exposure Time Point						Forward Primer	Reverse Primer	Dissociation Temperature (°C)
	Control	16 h	31 h	51 h	68 h	96 h			
Rhodopsin	0	−1.39	−2.44	−2.51	−1.83	−3.07	5′-GCTGAGCGCCACATCCA-3′	5′-AGGCACGTAGAATGCCGG-3′	81.8
Ash(a)	0	4.66	5.58	5.86	4.98	3.93	5′-GCCAGACGGAACGAGAGAGA-3′	5′-AGGGTTGCAAAGCCGTTG-3′	80.2
Stat3	0	3.02	3.04	1.91	2.3	1.83	5′-GAGGAGGCGTTTGGCAAA-3′	5′-TGTGTCAGGGAACTCAGTGTCTG-3′	81.8
Olig2	0	−0.39	−0.001	1.63	1.77	2.69	5′-GGAGGTCATGCCCTACGCT-3′	5′-GCAGCAGAGTGGCTATTTTAG-3′	82.4
Vimentin	0	−0.2	0.62	1.07	1.12	1.32	5′-ACTTTCTCCAGCCGGCAGTA-3′	5′-TAGTTGTAGGACGTGCGC-3′	84.5
Glutamine synthetase 1	0	−0.55	0.86	−0.25	−0.22	−0.26	5′-AGGATCGCCGCCCGT-3′	5′-TGCGAATTAGGGCCTCAGTG-3′	83
Carbonic anhydrase	0	−2.02	−1.72	−1.96	−1.3	−0.98	5′-GGAGAAGCTGCCAGTAAGCCT-3′	5′-TTGCAGCGCCGATCTTG-3′	80.2
Glial fibrillary acidic protein	0	1.54	1.59	1.5	2.27	1.91	5′-GCAGACAGGTGGATGGACTCA-3′	5′-GGCCAAGTTGTCTCTCTCGATC-3′	81.3
Green opsin	0	−4.74	−3.32	−1.96	−0.49	−1.2	5′-GGGAAGTAACACGCATGGTC-3′	5′-GCTGGCATAGGGAACCCA-3′	78.7
Glutamine synthetase 2	0	0.88	0.91	−0.22	−0.9	−0.97	5′-CGGCTGCCACACCAACTT-3′	5′-TCCTCAATATGCTTCAAACCTCC-3′	80.1
p27	0	0.19	−0.34	−0.3	−0.38	−0.13	5′-ACTGTAGGGTAACGGAGCAA-3′	5′-TTTTCCTCGGCTCTCGGA-3′	81.8
Pax6a	0	0.54	0.07	0.27	0.75	0.68	5′-CACATACACACCCCCGCAC-3′	5′-CCGAGGCGGCCATTG-3′	81.1

extended across the OPL into the ONL [Fig. 2(E,F) respectively]. In addition, large numbers of proliferating cells were present within the ONL at these times. Thus, by 31 h after light exposure initiation, INL cell proliferation began. This cell proliferation continued until maximal numbers of PCNA-positive progenitor cells were present in both the INL and ONL by 68 h. These larger numbers of proliferating cells persisted within these retinal layers through 96 h after light exposure initiation.

Time Course Analysis of Gene Expression in Light-Damaged Retinas by Microarray Hybridizations

The histological and immunohistochemical analyses from this and previous studies demonstrates that light-induced photoreceptor death initiates a dynamic retinal response during the first 96 h after initiating light treatment and ultimately results in the generation of new rod and cone photoreceptors (Vihtelic and Hyde, 2000; Vihtelic et al., 2005). To identify genes that play critical roles for photoreceptor regeneration, we performed a time course microarray experiment resulting in a gene set that included 4567 genes, of which 1677 showed an increase in their expression levels relative to the 0 h control (Supplemental data, Table 1).

As an initial validation of the microarray results, expression profiles for a small subset of genes identified from the microarray were independently analyzed by quantitative real-time PCR (qRT-PCR). Independent light lesion experiments were conducted and RNA was isolated from pooled retinas collected at the same time points examined using the microarray. Twelve different transcripts were selected for amplification at each of the time points (Table 1). For each of the genes examined, the relative expression level changes and the temporal pattern of these changes, as determined by qRT-PCR, mirrored the changes identified from the microarray (Table 1 and Fig. 3). This similarity in temporal expression patterns was observed for genes exhibiting decreased expression, such as the two *glutamine synthetase* genes, increased expression such as *gfap* (*glial fibrillary acidic protein*) and *stat3* (*signal transducer and activator of transcription 3*) and for genes with more complex expression patterns. Thus, the peak in *stat3* expression identified from the microarray at 16 h was verified by the qRT-PCR [Fig. 3(A,B)]. In addition, the dynamic temporal expression pattern of *olig2* (*oligodendrocyte lineage transcription factor 2*) was observed in both the microarray and the qRT-PCR

data [Fig. 3(A,B)]. These analyses demonstrate the integrity of the time course microarray analysis and the statistical methods used to produce the gene data set.

Cluster Analysis of Genes by Temporal Expression Profile and by Function

The data set of genes that exhibited significant expression level changes during the light exposure time course was further analyzed in two ways. First, the differentially expressed genes were grouped according to their expression profiles along the time series (Fig. 4 and Supplemental data, Table 2). GeneXplorer (Jiang et al., 2003), an interactive hierarchical clustering algorithm, was used to place each of the 4567 genes into one of 58 distinct temporal expression clusters [Fig. 4(A)]. Each cluster included genes exhibiting expression profiles similar to each other, but distinct from the genes in other clusters. In this analysis, a variety of expression patterns were identified, including ones that depicted gradually increasing expression levels, others that depicted early peaks of expression followed by decreasing expression levels, and still others that displayed delayed expression elevations [Fig. 4(B,C)]. These gene clusters may aid in identifying genes that function under similar regulatory controls.

The differentially expressed genes were also categorized by gene ontology. This analysis resulted in a large number of overlapping gene groups that were defined by various biological processes, molecular functions or cellular components (Table 2). The zebrafish genome sequence and its annotation are not complete and the UniGene build is still limited. Therefore, a proportion of the differentially expressed genes identified by the microarray hybridizations represents novel sequences and may not be associated with an ontological classification. In addition, several different proposed functions are often linked to the same gene based on sequence homology to various domains within the encoded protein. This results in the appearance of some genes in multiple ontology groups. In spite of this, these broad functional categories contained hundreds of identifiable genes and this analysis organized the data set into more specific functional groupings that could be managed more easily and analyzed by visual inspection. Furthermore, these groupings provided a broad depiction of the salient processes involved in the light-damage-induced photoreceptor regeneration. Thus, over 700 genes were identified with potential roles in cell metabolism, while fewer than 30 genes were clustered into the category of cell death. Similarly, greater than 500 gene products were associated with some form of catalytic activity, while 137 genes likely function in signal transduction. This gene ontology analysis also dissected the large data set into manageable groups and was a first step to generate hypotheses for the possible roles the various genes and their encoded proteins might play during light-induced retinal damage and the subsequent photoreceptor regeneration.

Hierarchical Clustering Within Functional Groups Identifies Up- and Down-Regulated Genes in the Regenerating Retinal Tissue

Several of these functional groups were selected for further analysis by hierarchical clustering of the differentially expressed genes in each group (Table 3, Fig. 5, and Supplemental data, Tables 3–10). The majority of genes in many of these groups were expressed at lower levels during the time course compared to their control levels. For example, $\sim$60% of genes that may function in cell communication, signal transduction, or transcription regulation were down-regulated. In contrast, most of the cell death, stress response, cell cycle and cell migration genes displayed increased transcript levels during this retinal response. Likewise, the expression levels for the majority of the calcium binding, cytoskeleton and proteasome complex genes identified in the microarray also increased. These distributions are consistent with the types of molecular processes thought to be necessary for initiating and regulating the regeneration response. Therefore, clusters of genes that may encode proteins with related functions during the different critical phases of this retinal regeneration response, including cell death, cell proliferation, cell migration and cell differentiation, were created based on visual inspection of these different ontological category gene lists and by further ontological analyses (Figs. 6 and 7, and Supplemental data, Figs. 1–4). Selected genes from the ontological groups that were composed of genes proposed to function in cell death, proliferation, migration and cell differentiation are described below.

Cell Death

Intense light causes photoreceptor apoptosis in both rodents and fish (Abler et al., 1996; Allen et al., 1999; Vihtelic and Hyde, 2000). Consequently, genes that regulate programmed cell death displayed changes in expression during this light damage time course [Fig. 6(A) and Supplemental data, Table 3 and Fig. 1]. These

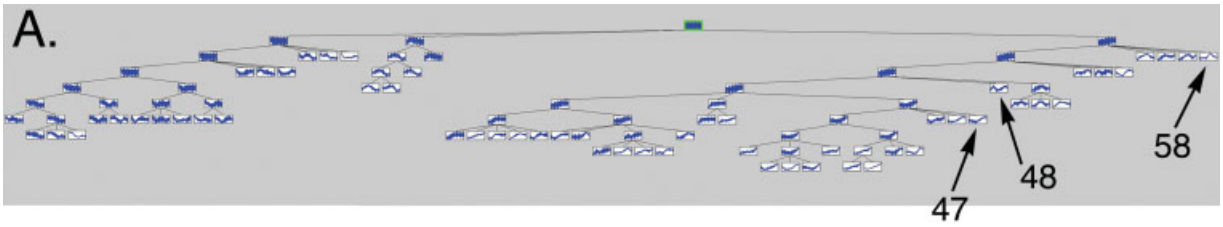

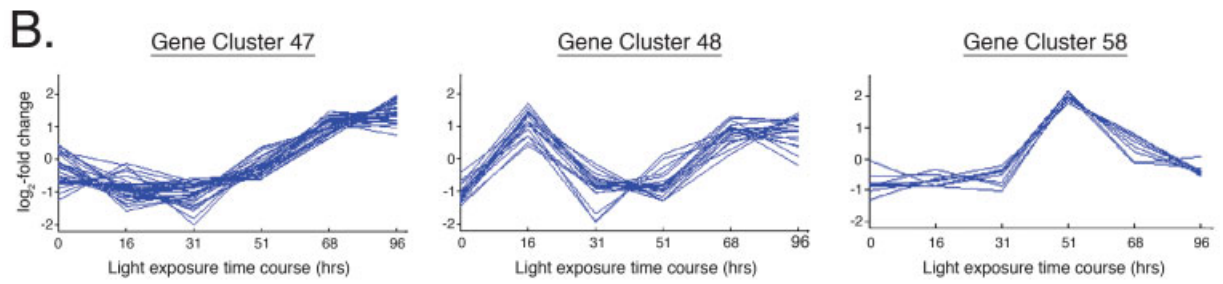

C.

Selected *Cluster 47* Genes

oligodendrocyte lineage transcription factor 2
CD9 antigen (p24)
glial fibrillary acidic protein
SEC22 vesicle trafficking protein-like
cathepsin L
cellular retinoic acid binding protein 1
hairy-related 4
dishevelled homolog 2
cyclin G2
synoretin
Rab-9

Selected *Cluster 48* Genes

follistatin
alphaB-crystallin
forkhead box K2
DNA methyl transferase 7
ankyrin-like protein 1
tumor-associated calcium signal transducer
synaptotagmin binding, RNA interacting protein
zinc transporter 6
apoptosis-inducing serine/threonine kinase 17b

Selected *Cluster 58* Genes

S-100 calcium binding protein
collagenase 3
lysyl oxidase
arylalkylamine N-acetyltransferase 1
KIHUCM creatine kinase
four and a half LIM domains a
ubiquitin-conjugating enzyme E2M
polyadenylate-binding protein-interacting protein 2

Figure 4

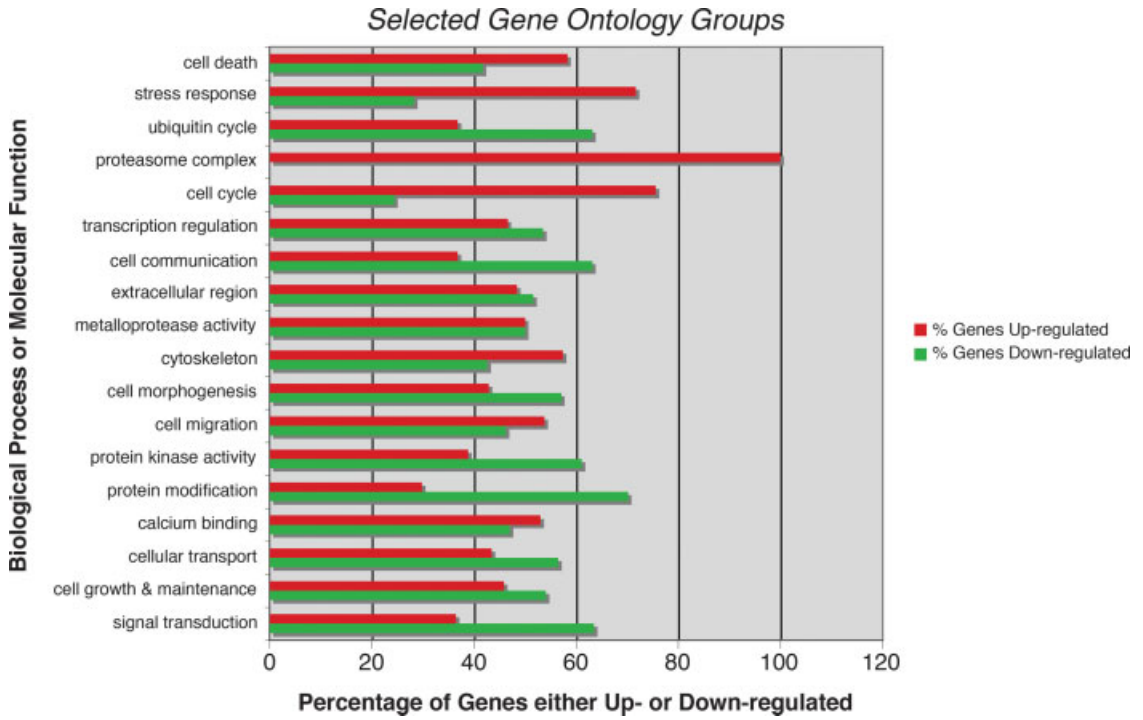

Figure 5

Table 2 Distribution of Differentially Expressed Genes by Ontology Category

Biological Process		Molecular Function		Cellular Component	
Ontology	Total Genes	Ontology	Total Genes	Ontology	Total Genes
Metabolism	755	nucleic acid binding	295	intracellular	485
Cell growth/maintenance	296	metal ion binding	196	nucleus	223
Stress response	46	protein binding	114	cytoplasm	216
Cell communication	174	catalytic activity	553	ribonucleoprotein complex	59
Cell death	24	transport activity	209	chromosome	17
Cell differentiation	20	signal transduction	137	ubiquitin ligase complex	14
Transcription regulation	159	transcription factor activity	86	integral membrane	149
Cell migration	26	protein kinase activity	59	plasma membrane	39
Morphogenesis	56	metallopeptidase activity	18	mitochondrial membrane	15
Embryonic development	24	calcium ion binding	83	inner membrane	9
Pattern specification	22	ubiquitin cycle	38	cytoskeleton	83
Protein modification	124	motor activity	16	proteasome complex	9
Cell cycle	45	structural molecule	82	extracellular region	31

included the *tumor necrosis factor receptor 21*, *bcl2-associated X protein* (*Bax*), *caspase 8*, *casp 8/FADD-like apoptosis regulator*, and *bcl2-like* genes, which were largely up-regulated at the earliest time point. In contrast, genes encoding a death effector domain-containing protein, brain-derived neurotrophic factor (BDNF), and Bcl2-related killer protein-like (Bok) displayed greatly reduced expression levels compared with the control. Interestingly, two Baculoviral IAP (inhibitor of apoptosis) repeat-containing genes (5a and 5b), which likely represent the zebrafish *survivin* paralogs, exhibited increased expression at the 68 and 96 h time points. In humans, Survivin expression is down-regulated in all tissues after development, but high expression levels are detected in various types of cancer (Grossman et al., 2001; Chiou et al., 2003; Kim et al., 2003).

Cell Proliferation

The increased cell proliferation, which occurs subsequent to the light-induced photoreceptor death, is a prominent and dramatic feature of this zebrafish regeneration response. Therefore, many cell cycle-related genes displayed expression changes during the time points examined in these experiments [Fig. 6(B) and Supplemental data, Table 4 and Fig. 2]. For example, at 31 h, when cell proliferation within the INL is beginning, increased levels of *mcm5* (*mini-chromosome maintenance 5*) were detected from the microarray hybridization [Fig. 6(B)]. High levels of *mcm5* transcripts were maintained during the time course. During development, the expression of *mcm5* correlates with the cell proliferation pattern in the zebrafish retina (Ryu et al., 2005; Ryu and Driever,

Figure 4 Temporal expression profile clusters. The 4567 genes that exhibited significant expression level changes during the time course were grouped according to their expression profiles along the time series. For this analysis, each gene was placed into one of 58 distinct expression clusters (A). The rooted diagram in (A) illustrates the hierarchical origins of the different gene clusters, which were progressively derived from the original gene set. The relative transcript level changes over the time course for individual genes in each cluster are displayed in graphical form as blue lines. Gene clusters 47, 48, and 58 are shown in greater detail as examples (B), with selected genes from each of these three clusters listed in Panel C.

Figure 5 Selected gene ontology groups. Genes within the data set were assigned to different ontology categories based on selected biological processes or molecular functions. These gene ontology groups were further analyzed by hierarchical clustering to determine if the genes displayed increased or decreased transcript levels during the time course. For each category, the red bar indicates the percentage of genes within that group that were up-regulated, while the green bar indicates the percentage of genes in the group that exhibited an overall reduction in expression during the time course.

Table 3 Selected Gene Ontology Groups

Category	Total Genes	Percentage Increased	Percentage Decreased
Cell death	24	41.7	58.3
Stress response	46	28.3	71.7
Ubiquitin cycle	38	63.2	36.8
Proteasome complex	9	0	100
Cell cycle	45	24.4	75.6
Transcription regulation	159	53.5	46.6
Cell communication	174	63.2	36.8
Extracellular region	31	51.6	48.4
Metallopeptidase activity	18	50	50
Cytoskeleton	47	42.6	57.4
Cell morphogenesis	56	57.1	42.9
Cell migration	26	46.2	53.8
Protein kinase activity	59	61.1	38.9
Protein modification	124	70.2	29.8
Calcium binding	83	47	53
Cellular transport	209	56.5	43.5
Cell growth and maintenance	296	54.1	45.9
Signal transduction	137	63.5	36.5

2006). The characterization of zebrafish *mcm5* mutants suggests this gene functions in a tissue-specific manner to regulate S phase duration and cell cycle exit (Ryu et al., 2005). Increased expression levels of *mcm3*, *mcm4*, and *mcm7* were also identified during the regeneration time course [Fig. 6(B)].

Immunohistochemistry demonstrated that individual PCNA-positive cells are evident in the ONL at 16 h and in the INL at 31 h (Fig. 2). Retinal progenitor amplification results in large numbers of PCNA-positive cell clusters in the INL and ONL at 51 through 96 h (Fig. 2). Similarly, the microarray analysis identified significant changes in PCNA transcript levels during the time course [Fig. 6(B)]. The increase in the PCNA transcript level roughly parallels the protein level changes, with the microarray suggesting a 2.3-fold increase in PCNA gene transcripts at 68 h compared to the control level (Supplemental data, Table 4).

A number of cyclin genes were also identified [Fig. 6(B)]. Based on the microarray, *cyclin B1* displayed the largest increase in transcription compared with the control, while *cyclin D1*, *cyclin F* and *cyclin E* expression also increased during the time course. In contrast, *cyclin E2* expression decreased. *Cyclin-dependent kinase inhibitor 1b* (*p27*, *kip1*) expression also decreased at 31 h, although *p57* gene expression displayed a gradual increase throughout the time course. Ubiquitin ligases such as *cullin 3* and *cullin 5*, which play critical roles in regulation of mitotic progression, were down-regulated during this retinal response. The differential regulation of these cell cycle-related genes likely occurs in both neuronal progenitors and in non-neuronal cells, such as the Müller glial and microglial cells within the light-damaged zebrafish retina (Wu et al., 2001; Faillace et al., 2002; Otteson and Hitchcock, 2003; Yurco and Cameron, 2005).

Cell Migration, Extracellular Matrix, and Cell Adhesion-Related Signaling

Re-establishment of the photoreceptor layer architecture depends on the directed migration of the newly generated retinal progenitor cells, and the properly regulated differentiation of the post-mitotic cells. In addition, photoreceptor regeneration likely initiates within the context of complex cellular reactions to the deafferentiation associated with the acute and widespread loss of the light-damaged rod and cone cells (Fisher et al., 2005). Non-neuronal cells, such as the Müller glia and microglia likely contribute in significant manners and may lend both positive and negative influences to the regeneration process (Lillo et al., 2001; Vihtelic et al., 2005; Yurco and Cameron, 2005). The directed migration of progenitor cells depends on both attractive and repulsive molecular influences that are conferred by both cell membrane and the extracellular matrix protein mix. Thus, chemokine receptor 4b (*cxcr4b*) expression increased, with highest transcript levels identified at 96 h [Fig. 6(C) and Supplemental data, Table 6 and Fig. 3]. In zebrafish, Cxcr4b plays a critical role in primordial germ cell migration and is localized within the membranes of these migrating cells (Doitsidou et al., 2002). In addition, the two zebrafish chemokine receptor genes (*cxcr4a* and *cxcr4b*) play essential roles in fin regeneration (Dufourcq and Vriz, 2006).

Genes encoding extracellular and matricellular proteins also displayed dynamic expression patterns in response to the intense light-induced insult [Fig. 6(C) and Supplemental data, Table 6 and Fig. 3]. For example, the highest levels of *matrix metalloproteinase 13* (*mmp13*) expression were identified during the initial stages of the response, while the *matrix metalloproteinase 2* (*mmp2*) expression increase was delayed until 68–96 h after light exposure intitiation [Fig. 6(C)]. The expression of *tissue inhibitor of metalloproteinase 2* (*timp2*) paralleled the *mmp2* transcript level increase. Tenascin C, an extracellular matrix molecule, which contributes to the environmental niche of neural stem cells and may function in neural stem cell migration and differentiation (Anstrom and

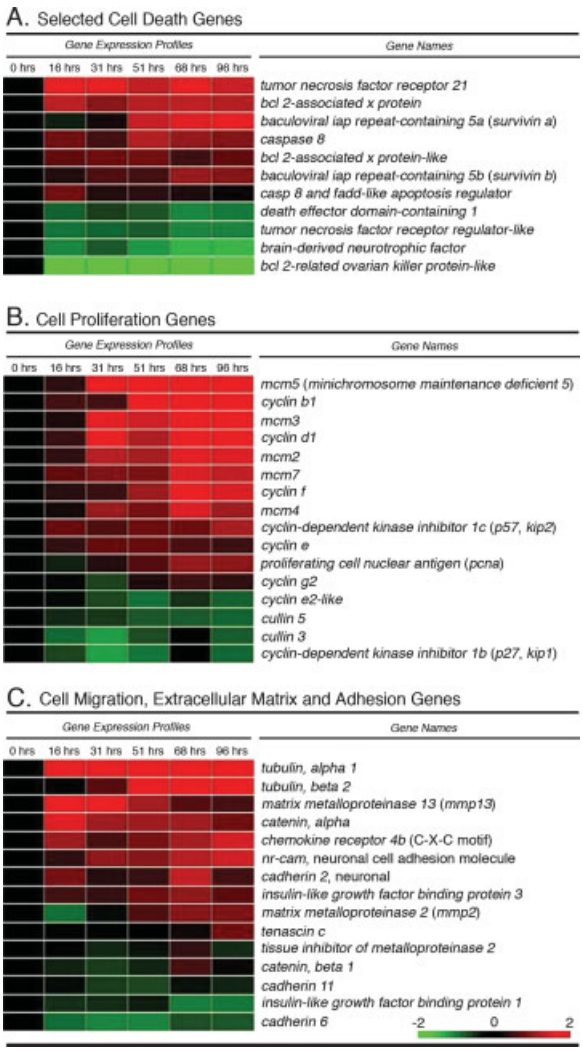

Figure 6 Expression profiles for selected genes within the cell death, cell proliferation and cell migration ontology groups. Subsets of genes encoding proteins involved in cell death (A), cell proliferation (B), and cell migration, extracellular matrix and adhesion (C) are shown. Heat maps for the selected genes and a scale are shown.

Tucker, 1996; Garcion et al., 2004), also increased at the 96 h time point [Fig. 6(C)]. In addition, *insulin-like growth factor binding protein 3* was highly expressed during the time course, while the *insulin-like growth factor binding protein 1* gene appeared to be down-regulated [Fig. 6(C)]. The genes encoding these insulin binding proteins are significant because Insulin-like growth factor 1 (IGF-1) regulates retinal progenitor proliferation in teleost retinas (Boucher and Hitchcock, 1998; Zygar et al., 2005).

Genes encoding cell adhesion and cell adhesion-related signaling proteins were also differentially regulated during this retinal regeneration response [Fig. 6(C)]. Neuronal *cadherin* (*cadherin 2*) transcript levels increased, while *cadherin 6* and *cadherin 11* levels significantly decreased compared to the non-light-treated control retinas. In addition, *nr-Cam* (a neuronal cell adhesion molecule) and *alpha catenin* transcript levels displayed rapid and sustained increases, while *beta catenin* transcript levels increased more modestly compared to the control. Genes encoding cytoskeletal components such as tubulins (α 1 and β 2) were also expressed at high levels compared with the controls during the time course [Fig. 6(C) and Supplemental data, Table 6 and Fig. 3].

Cell Differentiation and Signal Transduction

Proper regulation of rod and cone photoreceptor regeneration must rely on cell-cell signaling, intracellular signal transduction and various hierarchies of transcription factor expression. Consistent with these requirements, a variety of transcription regulators were identified from the microarray hybridizations (Fig. 7 and Supplemental data, Table 4 and Fig. 4). SRY-box containing genes such as *sox11b* and *sox4* were highly expressed during the time course compared to their control levels. In addition, helix-loop-helix genes such as *olig2* (*oligodendrocyte lineage transcription factor 2*) and *ath7* (*atonal homolog 7*) displayed increased expression, which was greatest at

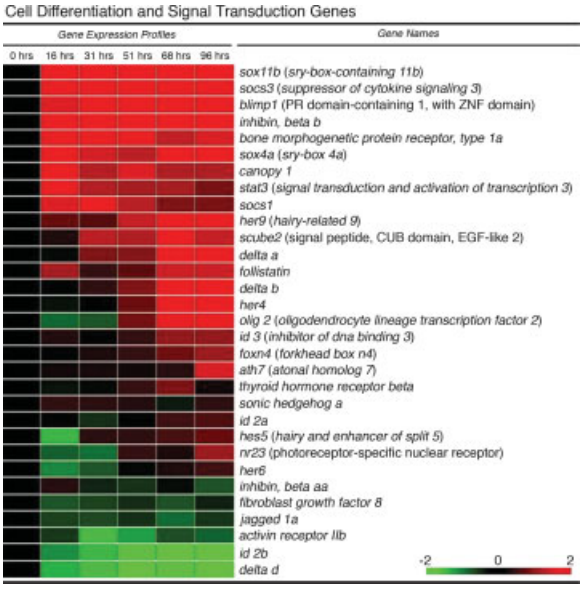

Figure 7 Expression profiles for selected cell differentiation and signal transduction genes. A subset of the statistically significant differentially expressed cell differentiation and signal transduction genes is shown. A scale for the heat maps is also shown.

the 68 and 96 h time points. These later time points are likely characterized by the expression of genes necessary for the commitment and differentiation of new photoreceptors. This is consistent with the increased expression at 96 h of a potential zebrafish ortholog of the photoreceptor-specific nuclear receptor gene [NR23; (Chen et al., 2005; Peng et al., 2005); Fig. 7 and Supplemental data, Table 4]. Likewise, the gene encoding thyroid hormone receptor beta (*trb*), which is necessary for green cone photoreceptor development in rodents (Ng et al., 2001), increased expression at 68 h compared to the control (Fig. 7).

Genes encoding negative regulators of neuronal differentiation such as the basic helix-loop-helix-containing proteins Id2a and Id3 were up-regulated in the regenerating retina, while *id2b* expression was dramatically reduced at all time points compared to the control level (Fig. 7). Notably, transcription factor genes that are important in photoreceptor cell commitment and differentiation during development such as *pax6b*, *six3a*, *six6*, *islet 1*, *dista-less homeobox 3b*, *cone-rod homeobox* and *retinal homeobox 1* were all down-regulated (Supplemental data, Table 4).

A number of hairy-related transcriptional repressors were also identified from the microarray analysis (Fig. 7). Genes such as *her9* and *her4* exhibited dramatically increased transcript levels, while *her8a*, *her6* and *hes5* only increased slightly during the time course (Fig. 7 and Supplemental data, Table 4 and Fig. 4). In addition, genes encoding the Notch ligands *delta A*, *delta B*, *jagged 1a* and *delta D* displayed significant transcript level changes compared to their control levels. These genes may function at the interface of neuron-glia fate decisions and their identification from the microarray analysis suggests a prominent role for Notch signaling pathways during the photoreceptor regeneration response (Campos et al., 2006; Yaron et al., 2006).

Bmp, Hedgehog and TGF-β-related signaling pathway members were also identified in this analysis. The *bone morphogenetic protein* (BMP) *receptor type 1a* gene was highly expressed during the time course (Fig. 7). Likewise, transcripts corresponding to the zinc finger transcriptional repressor *blimp1*, which encodes a PR domain-containing protein that inhibits chordin expression, were greatly elevated during the damage and regeneration response (Fig. 7). In zebrafish, *blimp1* is essential for proper development of the photoreceptor cell layer (Wilm and Solnica-Krezel, 2005).

Bmp signaling can have opposing influences on the Hedgehog signaling pathways during early development (Christian, 2000; Belecky-Adams and Adler, 2001; Adler and Belecky-Adams, 2002). In addition, Sonic Hedgehog plays critical roles during retinal development to regulate cell proliferation and differentiation (Stenkamp et al., 2000; Shkumatava and Neumann, 2005). The *scube2* gene, which encodes a secreted matrix protein that mediates Hedgehog signaling in the zebrafish embryo (Hollway et al., 2006), displayed increased expression levels in the regenerating retinas (Fig. 7). Likewise, the expression level of *sonic hedgehog* was slightly elevated compared with the control level (Fig. 7).

Genes encoding Activin members of the TGF-β superfamily also displayed significant expression level changes during the time course (Fig. 7). For example, *inhibin β B* and *follistatin* transcript levels increased, while *inhibin β A* and the *activin receptor IIb* transcript levels decreased during this time (Fig. 7). Similarly, *canopy 1*, a regulator of FGF signaling that interacts with FGFR1 (Hirate and Okamoto, 2006), exhibited greatly increased transcription, while *fgf 8* transcript levels were reduced compared to the control (Fig. 7).

The *signal transduction and activation of transcription* (*stat*) family genes were also differentially expressed during the light-damage-induced retinal response (Fig. 7 and Supplementary data, Table 10 and Fig. 4). For example, *stat3* expression increased over 6-fold compared with the control at the 16 h time point and relatively high expression levels persisted for the duration of the light exposure (Fig. 7 and Supplementary data, Table 10 and Fig. 4). Concomitant with the dramatic rise in *stat3* transcript levels, the expression of genes encoding inhibitors of Stat-mediated signaling also increased (Fig. 7). Thus, the increased expression levels of the Stat-induced Stat inhibitors 1 and 3 (*socs1* and *socs3*) paralleled the *stat3* transcript level dynamics in both magnitude and time course. The identification of high levels of transcription from both *stat3* and these Stat protein inhibitors strongly suggests the Stat3 transcription factor plays critical roles during this retinal response. Because of the large and rapid increase in *stat3* expression and previously identified roles for Stat3 in the regulation of retinal cell proliferation and differentiation (Zhang et al., 2004; Zhang et al., 2005), we felt this transcription factor was a good signaling candidate to have a potential role in the early retinal stem cell proliferation decision.

Stat3 Expression Increases Prior to Detectable INL Cell Proliferation

The Stat signaling pathways play wide ranging roles during development and tissue responses to stress.

For example, Stat3-mediated signaling is critical for rod photoreceptor development and Stat3 is activated in the rodent retina after exposure to bright light (Peterson et al., 2000; Zhang et al., 2004). In addition, Stat3 activation is associated with proliferating retinal precursor cells subsequent to cytokine treatment and may function to maintain the undifferentiated state of embryonic stem cells (Niwa et al., 1998; Matsuda et al., 1999; Zhang et al., 2005). Thus, it was not surprising that *stat3* transcription changed dramatically compared with the nonlight-treated control during both the early and later phases of this zebrafish retinal response. The *stat3* expression time course was verified by qRT-PCR (Fig. 3 and Table 1). In independent light lesion experiments, *stat3* transcripts increased more than 6-fold at 16 h compared with the control and *stat3* transcription remained elevated during the remaining time points.

We further examined Stat3 expression and activation by immunoblot and immunolocalization experiments. For these purposes, we generated rabbit polyclonal antiserum that recognizes zebrafish Stat3 and utilized two commercially available polyclonal antisera that each detect a different phosphorylated form of Stat3 (pStat-705 and pStat-727). Immunoblots of total retinal protein harvested from pooled retinas at the various time points from an independent light lesion experiment demonstrated that Stat3, pStat-705 and pStat-727 protein increased during the light exposure time course [Fig. 8(A)]. For these experiments, the same amounts of protein, based on the retinal extraction volumes, were loaded in each lane. In addition, the immunoblot signal intensities for the different Stat3 forms were normalized to the total actin protein levels (α-, β-, and γ-isoforms). Based on the immunoblots, the total actin protein levels in the light-lesioned retinas remained relatively constant during the time course, although the gene array data identified increased α- and β-actin transcript levels (data not shown). Low levels of Stat3 and the two different phosphorylated forms were detected in the control retinal extract [Fig. 8(A)]. Both Stat3 and pStat-727 protein increased steadily during the initial time points and peaked at 68 h, while pStat-705 protein levels peaked at 31 h [Fig. 8, compare (B) and (D) with (C)]. At 96 h, the levels of Stat3 and pStat-705 were both reduced compared their 68 h peak, but were still elevated relative to the control levels. Thus, the high level of *stat3* transcription, which was first identified in the microarray and verified by qRT-PCR, was followed by increased Stat3 protein translation. The time course of Stat3 phosphorylation parallels the protein translation and is consistent with the rapid activation of this transcription factor in response to the light-induced damage. Furthermore, the response persists during the phases of INL cell proliferation and cell differentiation.

Stat3 Expression in Proliferating Müller Glia

The spatial expression of Stat3 was determined by immunolocalization in frozen retinal sections (Fig. 9). In the control, Stat3 was detected at low levels within the distal INL, IPL and GCL [Fig. 9(A)]. At 16 h, Stat3 protein was identified in a small number of cells in the INL, the ganglion cell layer and in a few cells of the photoreceptor layer [Fig. 9(B), arrows, arrowheads, and asterisk, respectively]. At 31 h, the overall anti-Stat3 fluorescence intensity increased in the light-damaged retinas compared to the control, and a larger number of Stat3-expressing cells were present in the INL [Fig. 9, compare (C) with (A)]. This immunolocalization pattern persisted in the different retinal layers during the remaining time points (data not shown).

The location and morphology of the Stat3-positive cells at 16 and 31 h suggested the highest level of Stat3 in the INL was localized to the Müller glial cell nuclei. We employed a *gfap*:*EGFP* transgenic line that we generated, whose retinal EGFP expression is restricted to the Müller cells [Fig. 10(A–C)] to co-localize Stat3 expression. At 16 h of light exposure, the Stat3 signal within the INL was localized to the cell bodies of the Müller cells [Fig. 10(D–F)]. In addition, the Stat3-immunopositive cells did not correspond to amacrine cells as defined by HuC/D immunolocalization, although HuC/D-(+)/Stat3(+) ganglion cells were identified at 16 h light exposure [Fig. 10(G–I)].

Double immunolocalization of PCNA was used to identify Stat3-positive proliferating INL cells at 31 h of light exposure (Fig. 11). In this case, several of the Stat3-positive Müller cells [Fig. 11(A), arrows) also expressed PCNA [Fig. 11(B,C), arrows]. These data demonstrate the highest levels of Stat3 expression in the INL of the light-damaged regenerating zebrafish retina is localized to the Müller glia. In some cases, the Stat3 expression is associated with a proliferating subpopulation of these glial cells.

DISCUSSION

Constant intense light results in rod and cone photoreceptor cell death in *albino* zebrafish (Vihtelic and

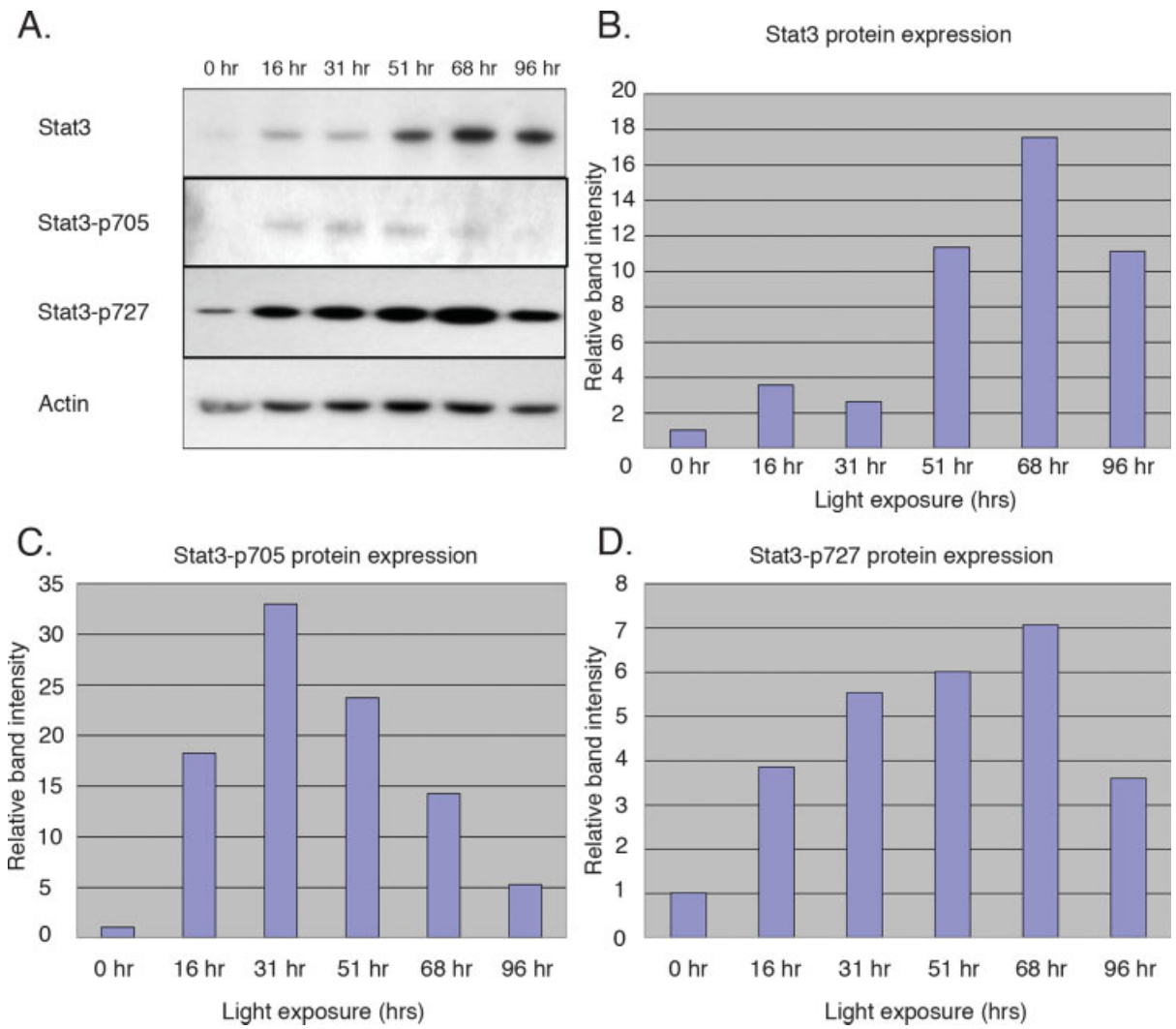

Figure 8

Hyde, 2000; Vihtelic et al., 2005). Regeneration of the different photoreceptor types is preceded by high levels of retinal cell proliferation, followed by progenitor cell migration from the INL to the ONL, commitment of the progenitors to the photoreceptor lineage and differentiation into rods or the appropriate cone cell types. Therefore, this regeneration response was conceptually divided into overlapping phases that were utilized as the framework for identifying genes that play critical roles during this process. Thus, the proliferation phase of the regeneration response is characterized initially by individual proliferating INL cells. This phase transforms to an amplification phase, which results in large numbers of INL cell clusters. Concomitant with this progenitor amplification, cells migrate from the INL to the ONL and new rod and cone photoreceptors differentiate from this precursor cell pool. We anticipated the microarray data would identify genes whose expression and function correspond to these processes and also genes with novel roles related to other significant

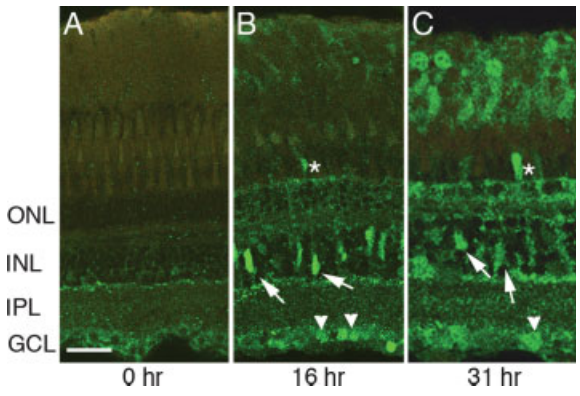

Figure 9

cell biological events occurring in the dynamic cellular environment of the damaged and regenerating retina.

Central to the strength of this study is our confidence in the integrity of the time course microarray analysis and of the statistical methods applied to the resulting data. Confidence in the precision of the array data is derived largely from two sources. First, several genes were represented multiple times ($n > 5$) on the array slides. The tight correspondence of expression levels for multiple replicates of these reporter genes indicates a high quality of experimental design and technical application (data not shown). Second, greater than 75% of the differentially expressed genes identified by ANOVA at the $p = 0.05$ significance level were also present at the $p = 0.01$ significance level. This suggests that the array data contains relatively clear delineations between differentially expressed and non-differentially expressed genes. When considered together, this suggests a good level of precision in the array data and validates the identification of differentially expressed genes.

Further, the accuracy of the array data was confirmed in two ways. First, qRT-PCR was performed on 12 genes that were identified as differentially expressed by the array analysis. The correspondence between the microarray and qRT-PCR level and pattern of expression for these genes further suggests the array data accurately represents the behavior of zebrafish genes during light-damage-induced photoreceptor regeneration (Table 1 and Fig. 3). Second, the cluster analysis of the microarray data is consistent with what is qualitatively expected for genes that may participate in the regeneration response. For example, the array analysis identified numerous genes potentially involved in the regulation of the cell cycle, cell migration, and neuronal differentiation (Figs. 6 and 7), events that have been documented to occur during the process of photoreceptor regeneration (Vihtelic and Hyde, 2000; Vihtelic et al., 2005). Thus, the precision of the array data is complemented by quantitative accuracy and qualitative representation of expected gene candidates that likely function in the experimentally defined phases of the regeneration response (Figs. 1 and 2; Vihtelic and Hyde, 2000; Vihtelic et al., 2005).

The raw microarray data were analyzed through several different methods. We normalized the fluorescence intensities on each array slide at each time point by the median intensity for each slide at each time point, respectively. This allowed for the uniform analysis of the data across the three array slide replicates. The subsequent $\log_2$-transformation ensured the data fit a normal distribution, which is a requirement for the application of the ANOVA tests. Further, the one-way ANOVA with the Bonferroni step-down procedure served as a moderate approach to identify differentially expressed genes (Holm, 1979). Alternative multiple testing corrections proved to be either too stringent, as with the Bonferroni correction, or too lenient, as with the Benjamini and Hochberg False Discovery Rate correction. The resulting large gene set may reflect the complexity of the damage and regeneration process and the desire to identify all the biologically significant genes at the potential expense of having a larger final gene set. Thus, while specific statistical analyses were chosen to fit the goals of this study, the integrity of the array data facilitated the application of a standard methodology: analyses were employed to normalize the data, remove data outliers, and identify genes exhibiting differential activity relative to the control samples.

Figure 8 Temporal expression of Stat3 protein. Polyclonal antisera to zebrafish Stat3 (Stat3) and two different Stat3 phosphorylated forms (Stat3-p705 and Stat3-p727) were used to label immunoblots of zebrafish retinal extracts (A). Total retinal proteins were harvested from non-light-lesion controls and at 16, 31, 51, 68 and 96 h of light exposure. Densitometric analysis of the immunoblots was used to quantify levels of Stat3, Stat3-p705 and Stat3-p727 during the time course (B–D, respectively). The densitometric determinations at each time point for the total Stat3 protein and the phosphorylated forms were normalized for the relative amount of protein loaded in each lane based on the Actin control shown in (A).

Figure 9 Immunolocalization of Stat3. The Stat3 polyclonal antiserum was used to label frozen retinal sections from control and light-lesioned fish. Low levels of Stat3 protein were detected in the IPL and GCL of the control (A), while increased anti-Stat3 signal is observed in the INL (arrows), GCL (arrowheads), and the ONL (asterisk) at 16 and 31 h of light exposure (Panels B and C). Abbreviations: ONL, outer nuclear layer; INL, inner nuclear layer; IPL, inner plexiform layer; GCL, ganglion cell layer. The scale bar represents 25 μm.

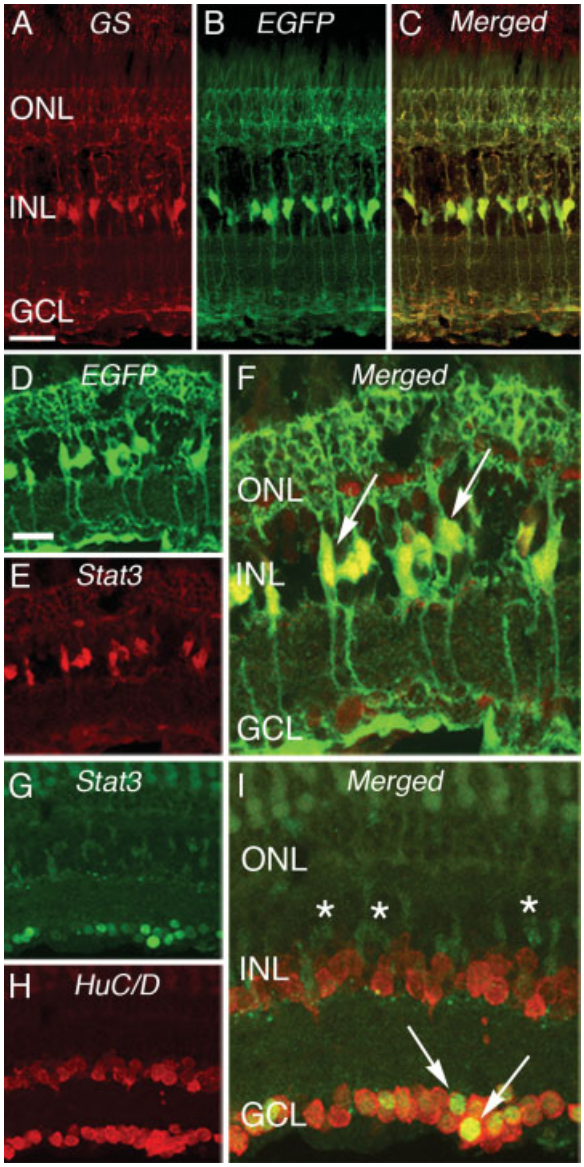

Figure 10 Stat3 expression in Müller glial cells. A transgenic line [*Tg*(*gfap:EGFP*)] expresses green fluorescent protein in zebrafish Müller cells (Panels A-C). Glutamine synthetase (red signal, A) in the Müller cells and EGFP expression in the transgenic line (green signal, B) are co-localized in the merged image (C). At 16 h of light exposure, EGFP-expressing Müller cells (green signal, D) also express Stat3 protein (red signal, E) within their nuclei in the INL (merged image, F, arrows). At 16 h of light exposure, Stat3-expressing cells (green signal, G and I, asterisks) co-localized with HuC/D-positive cells in the GCL (arrows, I), but not with the HuC/D-positive amacrine cells in the INL (red signal, H and I) as shown in the merged image (I). Abbreviations: ONL, outer nuclear layer; INL, inner nuclear layer; GCL, ganglion cell layer. The scale bar represents 25 μm.

We used two types of cluster analysis on the set of 4567 differentially expressed genes. First, we clustered the genes into 58 distinct groups based on their temporal expression profiles using the interactive hierarchical algorithm GeneXplorer. Numerous gene clustering algorithms have been developed in recent years, including K-Means clustering, the Self-Organizing Map, and various hierarchical approaches (Eisen et al., 1998; Alon et al., 1999; Tamayo et al., 1999; Tavazoie et al., 1999). However, these algorithms often suffer from high variability and low interactivity. For example, with each of these approaches, the particular organization of genes into clusters can change with each application of the algorithm and require user input of parameters that are not generally revealed. In addition, most clustering algorithms cannot integrate biological hypotheses or background knowledge that might otherwise help decide whether a cluster should be further divided or collapsed (Jiang et al., 2003). Thus, the robust grouping algorithm and the capability for user-interaction in GeneXplorer proved valuable in organizing our large gene set.

The clusters of co-expressed genes identified with GeneXplorer complemented the function-based clusters identified with GeneSifter. All of these clusters will become more valuable as annotation of the zebrafish genome sequence is completed. In addition, co-expressed genes may reveal functional or regula-

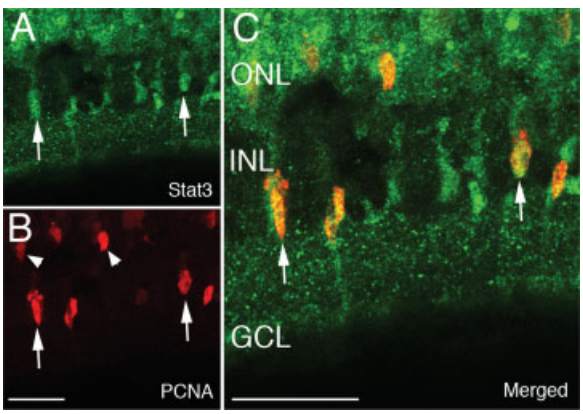

Figure 11 Stat3 and PCNA double immunolocalization. At 31 h of light exposure, Stat3-positive nuclei are observed in the INL (green signal, A, arrows). PCNA-positive cells are identified in the ONL and INL (red signal, B, arrowheads and arrows, respectively). The merged image (C) demonstrates the PCNA co-localizes within a subpopulation of Stat3-positive Müller cells (arrows). Abbreviations: ONL, outer nuclear layer; INL, inner nuclear layer; GCL, ganglion cell layer. Scale bars represent 25 μm.

tory similarities that can help generate hypotheses about relatively unknown genes. For example, gene clusters that exhibit related expression patterns may help identify coordinated transcriptional events. Moreover, the interactive features of GeneXplorer will facilitate more precise clustering as additional zebrafish genes are sequenced and annotated. This may result in the further division of some clusters that prove to include different functional groupings. Thus, functional and temporal gene clusters will accrue value as more is learned about the zebrafish genome and the molecular basis for regeneration of different retinal cell types as observed in the different retinal lesion paradigms.

A microarray experiment to identify gene expression changes during regeneration of the surgically-lesioned zebrafish retina was previously performed (Cameron et al., 2005). Gene expression was assayed at 2, 3, 5, and 14 days after the retinal lesion using an Affymetrix GeneChip® Zebrafish Genome Array, which is comprised of oligos corresponding to ~14,900 transcripts. The surgical lesion extends through the full-thickness of the retinal, RPE and choroid tissues, which results in the adjacent Müller cells proliferating and potentially regenerating all the retinal cell types (Yurco and Cameron, 2005). The light lesion model differs from the full-thickness retinal lesion paradigm in several ways. First, the light lesion data applies to the regeneration of a specific subset of retinal neurons (photoreceptors), while the surgical lesion data applies to the regeneration of all the different retinal cell types. This suggests the full-thickness retinal lesion may result in a more complex set of transcriptional changes necessary to regenerate the complete array of retinal neuronal cell types. Second, the regeneration response subsequent to light damage occurs across the entire central and dorsal parts of the retina, while the regeneration subsequent to the surgical lesion is restricted to the region adjacent to the lesion site, although the response may encompass up to 35% of the total retinal area (Cameron et al., 2005; Vihtelic et al., 2005). Therefore, the relative differences in transcript levels in the light-lesion model may be more robust than in the surgical damage model, allowing for greater detection of the differentially expressed genes. Finally, the cellular changes during light-damage-induced photoreceptor regeneration, as evidenced by histology and immunohistochemistry, occur over a much shorter time frame relative to the time course of the surgical lesion-induced response. The INL cell proliferation peaks at 72 h after light exposure initiation, while cell proliferation subsequent to the full-thickness retinal lesion achieves maximal levels at 7–14 days (Vihtelic and Hyde, 2000; Cameron et al., 2005; Vihtelic et al., 2005).

A detailed comparison between the gene expression profiles obtained using these two different retinal lesion paradigms is beyond the scope of this discussion, but identification of salient differences and similarities in the two data sets may be instructive. The early time points analyzed in the surgical lesion model represented the retinal response to acute injury (2, 3, and 5 days), while the 14-day post-lesion time point represented the regenerating retinal tissue (Cameron et al., 2005). Based on the reported analysis, increased levels of gene transcripts associated with macrophage activation, immune mechanisms and the cellular stress response were identified at 2, 3, or 5 days post-lesion; including complement C7 precursor, thioredoxin, and proteasome activator subunit transcripts. In comparison, the light-lesion model identified over 40 genes that may function in the cell stress response and a large number of proteasome- and ubiquitin-related genes (Fig. 5 and Supplemental data, Table 3). In addition, a group of cell death-related genes displaying both increased and decreased transcript levels over the time course were identified in the light-lesioned retinas (Figs. 5 and 6 and Supplemental data, Table 3). Genes in this functional category were not reported in the analysis of the surgically lesioned retina, although photoreceptor apoptosis occurs within 6 days post-lesion (Yurco and Cameron, 2005). These data are consistent with increased sensitivity in detection of differentially expressed genes afforded by the time course analysis subsequent to the light lesion.

A predominant gene ontology category identified at 14 days after the surgical lesion was cell cycle progression. Genes such as *regulator of cytokinesis 1*, *proliferation associated protein* (*p100*) and *activating transcription factor 3* displayed increased transcript levels compared to the control retinas, while *cyclin b1* and *tumor suppressor p53-binding protein 2* transcript levels were reduced. In comparison, transcripts for a variety of genes encoding cyclin proteins were also significantly increased in the light-treated retinas including *cyclin b1*, *cyclin d1*, *cyclin f*, and *cyclin e*, while *cyclin g2* and *cyclin e2-like* transcript levels were reduced compared to the control (Fig. 6 and Supplemental data, Table 4). The compact distribution of time points in the light-induced photoreceptor death and regeneration response, which differed in terms of only hours rather than days, may have allowed for greater sensitivity in *cyclin* gene identification compared to the retinal response to the surgical lesion. Similarly, a large number of Notch pathway ligands (and downstream effectors) displayed signifi-

cant transcript level changes during the photoreceptor regeneration time course. Various *notch* genes, including *notch 1a*, *notch 1b*, *notch 2*, and *notch 3*, displayed expression level changes during the time course; however, the statistical analysis precluded their inclusion in our final data set (data not shown). Examination of individual time points of the light-lesioned retina relative to the control, revealed a significant increase in *notch 3* transcript levels at the 68 h time point (data not shown). Similarly, *achaete scute homolog a* (*asha*), which displayed transcript level increases at 3 and 5 days in the surgical lesion model was also identified in the light-lesioned retina by analysis of individual time points (31, 51, 68 and 96 h; Table 1). Thus, some similarities in gene expression patterns were identified in the two microarray data sets. These preliminary comparisons between the two retinal regeneration data sets suggest that similar gene functional groups may play roles in the regeneration subsequent to both retinal damage paradigms.

This large-scale gene expression analysis has advantages over a mutational analysis where genes with unique functions are identified. The genome-wide microarray serves to identify genes that share similar functions during complex processes, such as photoreceptor regeneration. Therefore, this analysis can be utilized as a hypothesis-generating study. Based on models of neural stem cell regulation in the mammalian olfactory epithelium, which undergoes persistent neurogenesis like the teleost retina, a number of genes were identified in this microarray analysis that may play roles in stimulation of the retinal stem cells and the maintenance of a stem or progenitor cell niche. For example, secreted factors such as Follistatin, FGF8 and a number of BMPs function in a regulatory hierarchy within the olfactory epithelium and the underlying lamina propria to regulate proliferation and differentiation of olfactory receptor neurons (Beites et al., 2005). Similarly, genes encoding Follistatin, Inhibin β B, FGF8 and Canopy 1, a regulator of FGF receptor activity, all displayed dynamic expression changes during the photoreceptor regeneration response (Fig. 7). The requirements for both proneurogenic and antineurogenic activity must be properly balanced in the regenerating retina because high levels of BMP receptor gene expression (*bmpr1a*) and genes encoding a variety of Notch-related ligands were also identified in the microarray (Fig. 7). Likewise, the identification of *stat3* along with the *stat3* expression profile suggest possible models for function during the photoreceptor regeneration response, including early roles during INL cell proliferation initiation, and later tasks necessary for progenitor cell commitment and differentiation.

To explore potential functions for Stat3 during regeneration of the light-damaged photoreceptors, we generated anti-Stat3 polyclonal antiserum and examined the temporal and spatial expression of the Stat3 protein. As expected from the transcript level changes suggested by the microarray and verified by qRT-PCR, Stat3 expression increased during the time course (Fig. 8). In addition, levels of the activated phosphorylated forms of Stat3 also increased during the regeneration response (Fig. 8). Stat3 was immunolocalized to a subset of cells in the GCL and ONL, as well as the Müller glial cells (Figs. 9 and 10). Significantly, some of the Stat3-labeled Müller cells also expressed PCNA (Fig. 11). This demonstrates the Müller cells are actively proliferating during photoreceptor regeneration and likely represent the INL stem cells that have been proposed to regenerate photoreceptors, as well as other retinal cell types (Raymond and Hitchcock, 1997; Vihtelic and Hyde, 2000; Wu et al., 2001; Faillace et al., 2002; Yurco and Cameron, 2005; Fausett and Goldman, 2006; Raymond et al., 2006).

The early expression of Stat3 in Müller cells [Fig. 10(F)] may signify that Stat3 is one of the first genes up-regulated in these cells during regeneration. The co-localization of PCNA in a subset of the Stat3-labeled Müller cells appears to represent the initial Müller cell proliferation occurring in an asynchronous manner. Preliminary data in our lab suggests the Müller glia divide a limited number of times to produce a population of cells that expands between 51 and 68 h after light exposure initiation (data not shown). The expression of Stat3 in the majority of Müller cells at 16 h suggests its expression may be induced prior to the generation of the first neuronal progenitors from these glial cells. Stat3 expression during the initial stages of the proliferation response can be further analyzed in the context of the expression patterns of other genes identified from this analysis, such as *olig2*. Our preliminary data demonstrates that an *olig2:EGFP* transgene is expressed in either the Müller cells or neuronal progenitor cells at 68–96 h after light exposure initiation, but not in the Müller cells during the time that INL cell proliferation initiates at 31 h (unpublished data).

Unfortunately, the polyclonal antisera to the phosphorylated forms of Stat3 failed to generate a reproducible signal on tissue sections of the light-damaged regenerating retina (data not shown). This prevented the specific localization of activated Stat3 in the retinal tissue. However, the total Stat3 expression pattern determined using our polyclonal antiserum, correlates with the increased expression of the phosphorylated Stat3 forms, as demonstrated by immunoblots (Fig. 8). Therefore, we assume the increased expression of

total Stat3 overlaps both temporally and spatially with the increased expression of active Stat3.

Definitively determining roles of the Stat3 protein during zebrafish photoreceptor regeneration will require interference with activated Stat3 expression in the regenerating retina. We are developing an approach to conditionally knock-down gene expression at defined times during this regeneration response. This will allow us to test whether genes such as *stat3* are required to regulate processes such as cell proliferation, migration, or commitment. The identification of the *stat3* gene in the data set and the subsequent analysis of Stat3 protein expression demonstrates how this microarray-based gene expression analysis can be used to identify genes that will serve as candidates for being involved in particular aspects of retinal cell regeneration. Our subsequent analysis of the *olig2* gene further supports this usefulness. Detailed analysis of both the Stat3 and Olig2 proteins will be required to further understand their roles during the regeneration of photoreceptors and other retinal cell types.

Suzyanne Guzicki and the staff of Freimann Life Science Center provided zebrafish husbandry and care. We thank Peter Hitchcock for valuable discussions and advice.

REFERENCES

Abler AS, Chang C-J, Ful J, Tso MO. 1996. Photic injury triggers apoptosis of photoreceptor cells. Res Commun Mol Pathol Pharmacol 92:177–189.

Adler R, Belecky-Adams TL. 2002. The role of bone morphogenetic proteins in the differentiation of the ventral optic cup. Development 129:3161–3171.

Allen DM, Pipes C, Deramus K, Hallows TE. 1999. A comparison of light-induced rod degeneration in two teleost models. In: Hollyfield JG, Anderson RE, LaVail MM, editors. Retinal Degenerative Diseases and Experimental Therapy. New York: Kluwer Academic. p 337-350.

Alon U, Barkai N, Notterman DA, Gish K, Ybarra S, Mack D, Levine AJ. 1999. Broad patterns of gene expression revealed by clustering analysis of tumor and normal colon tissues probed by oligonucleotide arrays. Proc Natl Acad Sci USA 96:6745–6750.

Anstrom KK, Tucker RP. 1996. Tenascin-C lines the migratory pathways of avian primordial germ cells and hematopoietic progenitor cells. Dev Dyn 206:437–446.

Beites CL, Kawauchi S, Crocker CE, Calof AL. 2005. Identification and molecular regulation of neural stem cells in the olfactory epithelium. Exp Cell Res 306:309–316.

Belecky-Adams T, Adler R. 2001. Developmental expression patterns of bone morphogenetic proteins, receptors, and binding proteins in the chick retina. J Comp Neurol 430:562–572.

Boucher S-EM, Hitchcock PF. 1998. Insulin-related growth factors stimulate proliferation of retinal progenitors in the goldfish. J Comp Neurol 394:386–394.

Braisted JE, Essman TF, Raymond PA. 1994. Selective regeneration of photoreceptors in goldfish retina. Development 120:2409–2419.

Braisted JE, Raymond PA. 1992. Regeneration of dopaminergic neurons in goldfish retina. Development 114:913–919.

Cameron DA, Carney LH. 2000. Cell mosaic patterns in the native and regenerated inner retina of zebrafish: Implications for retinal assembly. J Comp Neurol 416:356–367.

Cameron DA, Easter SS. 1995. Cone photoreceptor regeneration in adult fish retina: Phenotypic determination and mosaic pattern formation. J Neurosci 15:2255–2271.

Cameron DA, Gentile KL, Middleton FA, Yurco P. 2005. Gene expression profiles of intact and regenerating zebrafish retina. Mol Vis 11:775–791.

Campos LS, Decker L, Taylor V, Skarnes W. 2006. Notch, epidermal growth factor receptor, and β1-integrin pathways are coordinated in neural stem cells. J Biol Chem 281:5300–5309.

Chen J, Rattner A, Nathans J. 2005. The rod photoreceptor-specific nuclear receptor Nr2e3 represses transcription of multiple cone-specific genes. J Neurosci 25:118–129.

Chiou SK, Jones MK, Tarnawski AS. 2003. Survivin—An anti-apoptosis protein: Its biological roles and implications for cancer and beyond. Med Sci Monit 9:PI25–P129.

Christian JL. 2000. BMP, Wnt and Hedgehog signals: How far can they go? Curr Opin Cell Biol 12:244–249.

Doitsidou M, Reichman-Fried M, Stebler J, Koprunner M, Dorries J, Meyer D, Esguerra CV, et al. 2002. Guidance of primordial germ cell migration by the chemokine SDF-1. Cell 111:647–659.

Dufourcq P, Vriz S. 2006. The chemokine SDF-1 regulates blastema formation during zebrafish fin regeneration. Dev Genes Evol 216:635–639.

Eisen MB, Spellman PT, Brown PO, Botstein D. 1998. Cluster analysis and display of genome-wide expression patterns. Proc Natl Acad Sci USA 95:14863–14868.

Faillace MP, Julian D, Korenbrot JI. 2002. Mitotic activation of proliferative cells in the inner nuclear layer of the mature fish retina: Regulatory signals and molecular markers. J Comp Neurol 451:127–141.

Fausett BV, Goldman D. 2006. A role for α1 tubulin-expressing Muller glia in regeneration of the injured zebrafish retina. J Neurosci 26:6303–6313.

Fisher SK, Lewis GP, Linberg KA, Verardo MR. 2005. Cellular remodeling in mammalian retina: Results from studies of experimental retinal detachment. Prog Retin Eye Res 24:395–431.

Garcion E, Halilagic A, Faissner A, ffrench-Constant C. 2004. Generation of an environmental niche for neural stem cell development by the extracellular matrix molecule tenascin C. Development 131:3423–3432.

Grossman D, Kim PJ, Blanc-Brude OP, Brash DE, Tognin S, Marchisio PC, Altieri DC. 2001. Transgenic expression of survivin in keratinocytes counteracts UVB-induced apoptosis and cooperates with loss of p53. J Clin Invest 108:991–999.

Hirate Y, Okamoto H. 2006. Canopy1, a novel regulator of FGF signaling around the midbrain-hindbrain boundary in zebrafish. Curr Biol 16:421–427.

Hitchcock P, Kakuk-Atkins L. 2004. The basic helix-loop-helix transcription factor neuroD is expressed in the rod lineage of the teleost retina. J Comp Neurol 477:108–117.

Hitchcock PF, Lindsey Myhr KJ, Easter SS Jr, Mangione-Smith R, Jones DD. 1992. Local regeneration in the retina of the goldfish. J Neurobiol 23:187–203.

Hitchcock PF, Raymond PA. 2004. The teleost retina as a model for developmental and regeneration biology. Zebrafish 1:257–271.

Hollway GE, Maule J, Gautier P, Evans TM, Keenan DG, Lohs C, Fischer D, et al. 2006. Scube2 mediates Hedgehog signalling in the zebrafish embryo. Dev Biol 294: 104–118.

Holm S. 1979. A simple sequentially rejective Bonferroni test procedure. Scand J Stat 6:65–70.

Jiang D, Pei J, Zhang A. 2003. Towards interactive exploration of gene expression patterns. SIGKDD Explorations 5:79–90.

Johns PR. 1977. Growth of the adult goldfish eye. III. Source of the new retinal cells. J Comp Neurol 176:343–358.

Johns PR. 1982. Formation of photoreceptors in larval and adult goldfish. J Neurosci 2:178–198.

Johnson MR, Wang K, Smith JB, Heslin MJ, Diasio RB. 2000. Quantitation of dihydropyrimidine dehydrogenase expression by real-time reverse transcription polymerase chain reaction. Anal Biochem 278:175–184.

Julian D, Ennis K, Korenbrot JI. 1998. Birth and fate of proliferative cells in the inner nuclear layer of the mature fish retina. J Comp Neurol 394:271–282.

Kawakami K, Koga A, Hori H, Shima A. 1998. Excision of the tol2 transposable element of the medaka fish, Oryzias latipes, in zebrafish, Danio rerio. Gene 225:17–22.

Kim PJ, Plescia J, Clevers H, Fearon ER, Altieri DC. 2003. Survivin and molecular pathogenesis of colorectal cancer. Lancet 362:205–209.

Lillo C, Velasco A, Jimeno D, Cid E, Aijon J, Lara JM. 2001. Non-neuronal cells involved in the degeneration and regeneration of the fish retina. J Neurocytol 30:475–491.

Matsuda T, Nakamura T, Nakao K, Arai T, Katsuki M, Heike T, Yokota T. 1999. STAT3 activation is sufficient to maintain an undifferentiated state of mouse embryonic stem cells. EMBO J 18:4261–4269.

Ng L, Hurley JB, Dierks B, Srinivas M, Salto C, Vennstrom B, Reh TA, et al. 2001. A thyroid hormone receptor that is required for the development of green cone photoreceptors. Nat Genet 27:94–98.

Niwa H, Burdon T, Chambers I, Smith A. 1998. Self-renewal of pluripotent embryonic stem cells is mediated via activation of STAT3. Genes Dev 12:2048–2060.

Otteson DC, D'Costa AR, Hitchcock PF. 2001. Putative stem cells and the lineage of rod photoreceptors in the mature retina of goldfish. Dev Biol 232:62–76.

Otteson DC, Hitchcock PF. 2003. Stem cells in the teleost retina: Persistent neurogenesis and injury-induced regeneration. Vision Res 43:927–936.

Peng GH, Ahmad O, Ahmad F, Liu J, Chen S. 2005. The photoreceptor-specific nuclear receptor Nr2e3 interacts with Crx and exerts opposing effects on the transcription of rod versus cone genes. Hum Mol Genet 14:747–764.

Peterson WM, Wang Q, Tzekova R, Wiegand SJ. 2000. Ciliary neurotrophic factor and stress stimuli activate the Jak-STAT pathway in retinal neurons and glia. J Neurosci 20:4081–4090.

Raymond PA, Barthel LK, Bernardos RL, Perkowski JJ. 2006. Molecular characterization of retinal stem cells and their niches in adult zebrafish. BMC Dev Biol 6: 36.

Raymond PA, Hitchcock PF. 1997. Retinal regeneration: Common principles but a diversity of mechanisms. In: Seil FJ, editor. Advances in Neurology. Philadelphia, PA: Lippincott-Raven. pp 171–184.

Raymond PA, Reifler MJ, Rivlin PK. 1988. Regeneration of goldfish retina: Rod precursors are a likely source of regenerated cells. J Neurobiol 19:431–463.

Ryu S, Driever W. 2006. Minichromosome maintenance proteins as markers for proliferation zones during embryogenesis. Cell Cycle 5:1140–1142.

Ryu S, Holzschuh J, Erhardt S, Ettl AK, Driever W. 2005. Depletion of minichromosome maintenance protein 5 in the zebrafish retina causes cell-cycle defect and apoptosis. Proc Natl Acad Sci USA 102:18467–18472.

Shkumatava A, Neumann CJ. 2005. Shh directs cell-cycle exit by activating p57Kip2 in the zebrafish retina. EMBO Rep 6:563–569.

Stenkamp DL, Frey RA, Prabhudesai SN, Raymond PA. 2000. Function for Hedgehog genes in zebrafish retinal development. Dev Biol 220:238–252.

Tamayo P, Slonim D, Mesirov J, Zhu Q, Kitareewan S, Dmitrovsky E, Lander ES, et al. 1999. Interpreting patterns of gene expression with self-organizing maps: Methods and application to hematopoietic differentiation. Proc Natl Acad Sci USA 96:2907–2912.

Tavazoie S, Hughes JD, Campbell MJ, Cho RJ, Church GM. 1999. Systematic determination of genetic network architecture. Nat Genet 22:281–285.

Thummel R, Burket CT, Brewer JL, Sarras MP Jr, Li L, Perry M, McDermott JP, et al. 2005. Cre-mediated site-specific recombination in zebrafish embryos. Dev Dyn 233: 1366–1377.

Vihtelic TS, Doro CJ, Hyde DR. 1999. Cloning and characterization of six zebrafish photoreceptor opsin cDNAs and immunolocalization of their corresponding proteins. Vis Neurosci 16:571–585.

Vihtelic TS, Hyde DR. 2000. Light-induced rod and cone cell death and regeneration in the adult albino zebrafish (*Danio rerio*) retina. J Neurobiol 44:289–307.

Vihtelic TS, Soverly JE, Kassen SC, Hyde DR. 2005. Retinal regional differences in photoreceptor cell death and regeneration in light-lesioned albino zebrafish. Exp Eye Res 82:558–575.

Vong QP, Chan KM, Cheng CH. 2003. Quantification of common carp (*Cyprinus carpio*) IGF-I and IGF-II mRNA by real-time PCR: Differential regulation of expression by GH. J Endocrinol 178:513–521.

Westerfield M. 1993. The Zebrafish Book. Eugene, OR: University of Oregon Press.

Wilm TP, Solnica-Krezel L. 2005. Essential roles of a zebrafish prdm1/blimp1 homolog in embryo patterning and organogenesis. Development 132:393–404.

Wu DM, Schneiderman T, Burgett J, Gokhale P, Barthel L, Raymond PA. 2001. Cones regenerate from retinal stem cells sequestered in the inner nuclear layer of adult goldfish retina. Invest Ophthalmol Vis Sci 42:2115–2124.

Yaron O, Farhy C, Marquardt T, Applebury M, Ashery-Padan R. 2006. Notch1 functions to suppress cone-photoreceptor fate specification in the developing mouse retina. Development 133:1367–1378.

Yurco P, Cameron DA. 2005. Responses of Muller glia to retinal injury in adult zebrafish. Vision Res 45:991–1002.

Zhang SS, Liu MG, Kano A, Zhang C, Fu XY, Barnstable CJ. 2005. STAT3 activation in response to growth factors or cytokines participates in retina precursor proliferation. Exp Eye Res 81:103–115.

Zhang SS, Wei J, Qin H, Zhang L, Xie B, Hui P, Deisseroth A, et al. 2004. STAT3-mediated signaling in the determination of rod photoreceptor cell fate in mouse retina. Invest Ophthalmol Vis Sci 45:2407–2412.

Zygar CA, Colbert S, Yang D, Fernald RD. 2005. IGF-1 produced by cone photoreceptors regulates rod progenitor proliferation in the teleost retina. Brain Res Dev Brain Res 154:91–100.